Investigations on Flow Behavior Inside the Compartments of Electrodialysis(ED) Stack

By

Bhavesh K. Patel

09MMET10

DEPARTMENT OF MECHANICAL ENGINEERING

INSTITUTE OF TECHNOLOGY

NIRMA UNIVERSITY

AHMEDABAD-382481

MAY 2011

Investigations on Flow Behavior Inside the Compartments of Electrodialysis(ED) Stack

Major Project

Submitted in partial fulfillment of the requirements

For the degree of

Master of Technology in Mechanical Engineering (Thermal)

By

Bhavesh K. Patel

09MMET10

DEPARTMENT OF MECHANICAL ENGINEERING

INSTITUTE OF TECHNOLOGY

NIRMA UNIVERSITY

AHMEDABAD-382481

MAY 2011

Declaration

This is to certify that

i) The thesis comprises my original work towards the degree of Master of Technology in Mechanical Engineering (Thermal) at Nirma University and has not been submitted elsewhere for a degree.

ii) Due acknowledgement has been made in the text to all other material used.

Bhavesh K. Patel

Certificate

This is to certify that the Major Project entitled "Investigations on Flow behavior inside the compartments of Electrodialysis(ED) stack" submitted by Bhavesh K. Patel (09MMET10), towards the partial fulfillment of the requirements for the degree of Master of Technology in Mechanical Engineering (Thermal) of Nirma University of Science and Technology, Ahmedabad is the record of work carried out by him under my supervision and guidance. In my opinion, the submitted work has reached a level required for being accepted for examination. The results embodied in this major project, to the best of my knowledge, haven't been submitted to any other university or institution for award of any degree or diploma.

Dr. Girish. R. Desale
External Guide,
Scientist,
Workshop Superintendent,
Design Drawing,Workshop Engg. Dept.,
CSMCRI,Bhavnagar.

Dr. V. J. Lakhera
Project Guide,
Professor,
Department of Mechanical Engineering,
Institute of Technology,
Nirma University, Ahmedabad.

Prof. V. R. Iyer
Professor and Head,
Department of Mechanical Engineering,
Institute of Technology,
Nirma University, Ahmedabad

Dr K Kotecha
Director,
Institute of Technology,
Nirma University, Ahmedabad

Abstract

Electro dialysis (ED) is one of the electrically driven process using ion-exchange membranes which has been developed for several years, mainly for desalting of brackish water and sea water. ED process is now days used for separation of chemicals from a mixture of ionic and non ionic substances. The ED stack is generally used in various industrial processes namely, water purification, effluent treatment, desalination of chemicals, recovery of valuable chemicals, etc. In ED process, the flow of chemical over the surface of the membrane plays an important role in overall efficiency, the performance and the energy consumption etc. That determines the product cost of chemicals and ultimately the capital cost.

In a ED unit, the compartments are formed by alternate arrangement of cation and anion exchange membranes. The arrangement of compartments play a vital role for equal distribution of liquid in the compartments. There are mainly three different types of arrangements adopted in a ED stack: (1) Parallel flow pattern, (2) Series flow pattern, and (3) Parallel-cum- series flow pattern. The arrangement of compartments in parallel and group of parallel compartments in series (parallel-cum-series) is preferred for handling huge amount of liquid in the ED stacks. The present investigation has been conducted by taking a parallel-cum-series pattern in the existing ED unit.

For the design optimization of the stack and compartment, the parameters are namely, the inlet and outlet openings and the effective area (contact area of water flow with membrane) of membrane. The water inside the compartment flows in narrow streams due to the path of least resistance which leads to high velocity of the water jet. Due to this, its covers the less area of membrane and ions will not have sufficient time to get transported from treated compartment to rejected one. Thus for the improvement in the design of the ED stack and its compartments, the inlet and outlet openings are mainly responsible for the effective flow distribution in stack and compartments which significantly improves the transportation of ions and hence

the performance of the ED unit. From the literature review pertaining to parallel-cum-series arrangement, it was noted that there was a possibility of an uneven fluid flow through the compartments and hence a lesser efficient system. The present work is an attempt to ascertain the flow behaviour inside an existing ED stack and the compartments in each stage of the unit. Further, investigations have been made with new proposed design aspects adopted in an Electro dialysis unit viz. the inlet header design, and, design of compartment inlet and outlet openings in order to improve its performance and efficiency.

As the ED stack is a closed system hence it is very difficult to observe the flow inside the compartments and in the stack itself. Hence CFD (Computational Fluid Dynamics) is the most effective tool to analyze the flow behaviour and its pattern inside the compartment. The theoretically calculated flow velocity and pressure and are found to conform to the value predicted by using FLUENT software. The flow patterns inside the ED stack and the compartments (with existing and new proposed design) observed experimentally are found to conform to the flow patterns observed in FLUENT.

Acknowledgements

I take this opportunity to express my deep sense of gratitude to my esteemed supervisor Dr. G.R Desale, Scientist and Workshop Superintendent, Design Drawing and Workshop Engineering Department, Central Salt And Marine Chemicals Research Institute (CSMCRI), Bhavnagar, Gujarat, and to my guide Dr. V. J Lakhera, Mechanical Engineering Department, Institute of Technology, Nirma University, for their keen interest, constant encouragement and valuable guidance at all stages of this dissertation work. I am also grateful Dr. S.K Thampy, Scientist, CSMCRI Bhavnagar, Dr. R.N Patel, Cordinator M.Tech Thermal Engineering program, Institute of Technology, Nirma University, Ahmedabad.

I am also thankful to Dr. P.K Ghosh,Director,CSMCRI,Bhavnagar,for allowing me to carry out this work at their premises. I am also thankful to Prof. V.R Iyer, Head of Mechanical Engineering Department for allowing me to undertake this work and for their guidelines during the review process.This work could not be completed without the support and co-ordination of Mr. Nitin G Borle, Technician Group-Two of the Design and Workshop Engineering Department,CSMCRI, Bhavnagar. It is a pleasure to acknowledge the co-operation of all the staff member of CSMCRI,Bhavnagar.

I would like to thank my friends- Darshan, Keran and Hemang for sharing their enthusiasm and kind support during work. I would also thank my parents,brother and sister. They were always supporting me and encouraging me with their best wishes.

- Bhavesh K Patel
09MMET10

Contents

List of Figures

Chapter 1

Introduction

1.1 General

Water is of great importance in any industrial, domestic and agricultural consumption so that its shortage is one of the most important limitations of life, agriculture and industries. Most of the earth's surface is covered by water, which is in the form of the oceans, the seas and the ice in the poles. However, only 1% of these waters which are in the form of surface or underground water is used by human beings and that is because the water of the oceans and the seas has a very high salt content and it is not directly utilizable and therefore it needs some special processes to be desalinated [4]. Suitable desalinating methods for water treatment of seawater can be effective to overcome the water shortage. Different processes involved for the desalination and purification are shown in table-1 with their basic applications.

Electrodialysis (ED) is one of these methods which has been used for many years in different branches of industry for water treatment, in particular, for producing deionized water of high purity, and drinking water. ED is an electrochemical process for the separation of ions across charged membranes from one solution to another under the influence of an electrical potential difference used as a driving force. This

Table I: Different processes for desalination and its applications

State-of-the-art processes	**Technical relevant applications**
Electrodialysis	Water desalination and salt pre-concentration
Diffusion dialysis	Acid and base recovery from industrial waste waters
Donnan dialysis	Water softening, and exchange of ions
Developing processes	**Technical relevant applications**
Bipolar membrane electrodialysis	Production of acids and bases from salts
Continuous electrodeionization	Production of ultra pure water
Capacitive deionization	Water desalination and water softening
Reverse electrodialysis	Electrodialytic energy generation

process has been widely used for production of drinking and process water from brackish and seawater, treatment of industrial effluents, recovery of useful materials from effluents and salt production. The basic principles of ED as shown in Fig.1.1 have been reviewed in the literature [5].

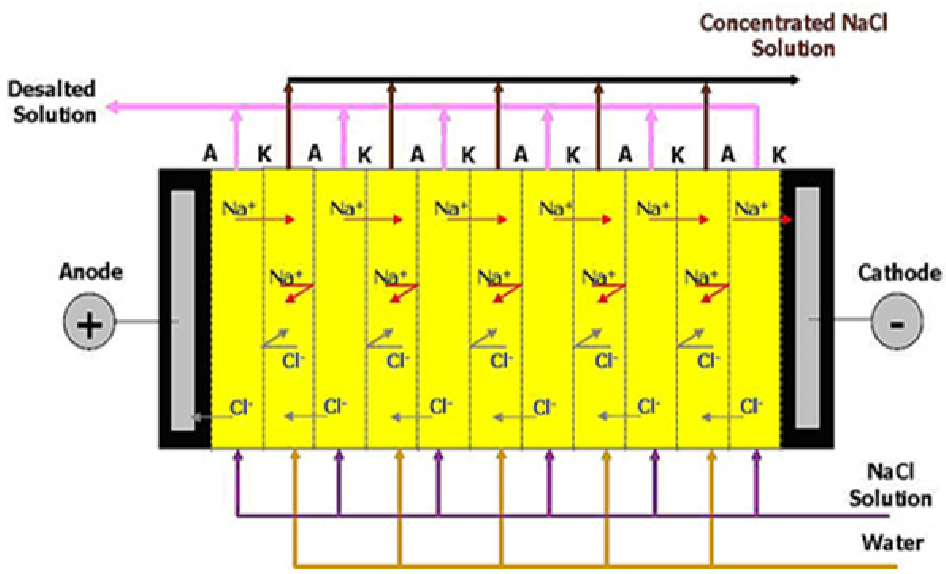

Figure 1.1: Basic principle of Electrodialysis

In a typical ED cell, a series of anion- and cation-exchange membranes are arranged in an alternating pattern between an anode and a cathode to form individual cells as shown in Fig.1.2. When a DC potential is applied between two electrodes, positively charged cations move toward the cathode, pass through the negatively charged cation-exchange membrane and are retained by the positively charged anion-exchange membrane. On the other hand, negatively charged anions move toward the anode, pass through the positively charged anion-exchange membrane and are retained by the negatively charged cation-exchange membrane. At the end, ion concentration increases in alternate compartments with a simultaneous decrease of ion concentration in other compartments. A schematic view of an ED cell Pair is presented in Fig.1.2 and and combined cell pairs form an Electrodialysis unit is shown Fig.1.3.

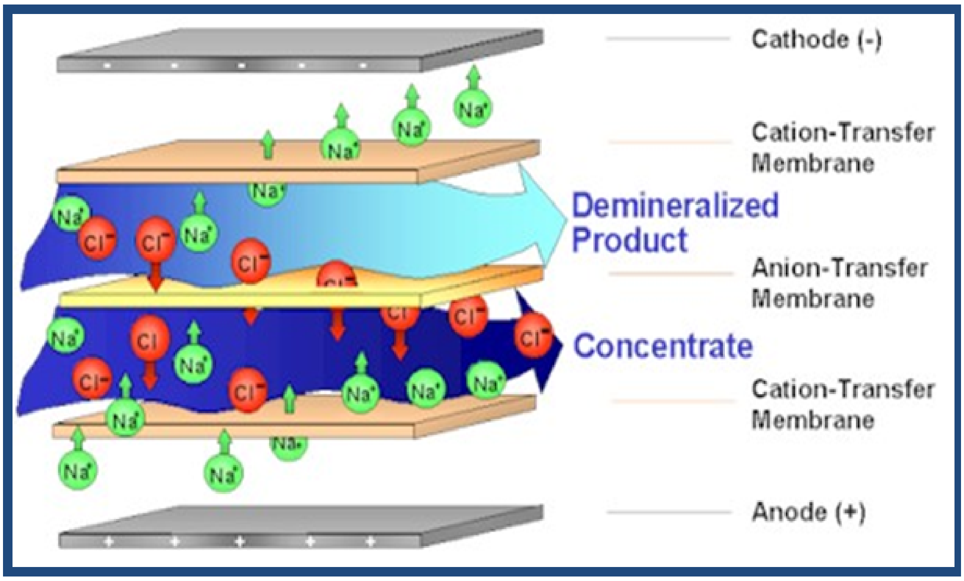

Figure 1.2: A single Cell Pair

In order to improve the performance of an electrodialyzer, a lot of investigations are performed as exemplified below. Ions transferring across the membrane are supplied from a feeding solution, accordingly the performance of an electrodialyzer is influenced by the solution flow in desalting cells. For accelerating the ionic transport from the solution toward the membrane, theoretical and experimental study of hydrodynamics of the solution flow is carried out. Limiting current density is caused by concentration polarization in a boundary layer formed at a desalting surface of the membrane.

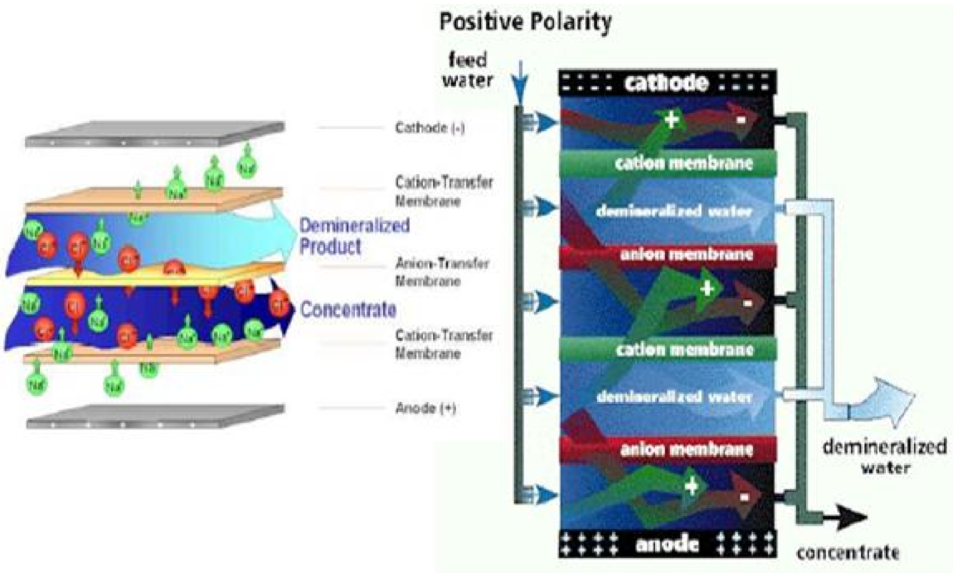

Figure 1.3: ED stack and Processes involved

This parameter is usually measured by current density-voltage curves. The mechanism of the limiting current density is analyzed based on the mass transport in a desalting cell by means of chemical engineering techniques. Further, electrodialysis is applied to remove specified ionic species in a feeding solution due to permselectivity of the membranes. Based on the fundamental studies exemplified above, the electrodialysis process is applied widely to the desalination of brackish water[6].

1.2 Various applications of Electrodialysis water are given as below

a. Desalting seawater

b. Large scale brackish and seawater desalination and salt production.

c. Small and medium scale drinking water production (e.g., towns and villages, construction and military camps, nitrate reduction, hotels and hospitals)

d. Water reuse (e.g.,industrial laundry waste water, produced water from oil/gas production, cooling tower makeup and blowdown, metals industry fluids, wash-rack water)

e. Pre-demineralization (e.g., boiler makeup and pretreatment, ultrapure water pretreatment, process water desalination, power generation, semiconductor, chemical manufacturing, food and beverage)

f. Treating brackish groundwater

g. Water softening

h. Waste water recovery

i. Removing color, odor, and other organic contaminants

j. Chemical sepration and solution demineralization

k. Bipolar-membrane electrodialysis was oriented toward the recovery of acids and bases from salt streams.

1.3 Limitations

a. Working best at removing low molecular weight ionic components from a feed stream. Non-charged, higher molecular weight, and less mobile ionic species will not typically be significantly removed.

b. In contrast to RO, electrodialysis becomes less economical when extremely low salt concentrations in the product are require.

c. Consequently, comparatively large membrane areas are required to satisfy capacity requirements for low concentration (and sparingly conductive) feed solutions.

d. As with RO, electrodialysis systems require feed pretreatment to remove species that coat, precipitate onto, or otherwise ”foul” the surface of the ion exchange membranes. This fouling decreases the efficiency of the electrodialysis system.

e. Electrodialysis reversal systems seek to minimize scaling by periodically reversing the flows of diluate and concentrate and polarity of the electrodes

f. The most hazardous for electrodialysis are hardness salts, especially calcium salt.

g. In an electrodialysis process, energy consumption is rather high comparing to a reverse osmosis process when a high concentration solution such as seawater is supplied.

Overall current efficiencies of less than unity are due to a number of contributing factors[7]

a. the membranes may not have a permselectivity of unity and therefore allow passage (intrusion) of the co-ion.

b. parallel currents may exist across the membrane stack manifbld (current leakage).

c. at high current densities or low solute concentrations, hydrogen and hydroxide ions present in the aqueous media begin to participate in the current carrying process (transport by water dissociation ions).

d. the concentration gradient across a membrane separating the diluate and concentrate compartments drives a diffusive flux of electrolyte back into the diluate (counterion backdiffusion).

1.4 Involvement of CFD approach

The process/technique used in desalination involves lots of fluid mechanics and its applications. The nature of fluid flow is complex and could not be analyzed using simple mathematical equations and hence computational fluid dynamics (CFD) is extensively used by many investigators. The development of the high speed computer and the evolution of the computational fluid dynamics (CFD) have a great influence on the engineering design and analysis of the turbo machinery. In the past decades, due to increasing capability to solve complex geometry and complex flow problems and reduction in computational time and costs, the CFD methodology has emerged to become an efficient approach for collecting information to improve engineering design of turbo machinery. Today, CFD is an equal partner with pure theory and pure experiment in the analysis and solution of fluid dynamics problem. And CFD will continue to play this role indefinitely, for as long as our advanced human civilization exists. The fundamental basis of almost all CFD problems is the Navier-Stokes equations, which define any single-phase fluid flow. These equations can be simplified by removing terms describing viscosity to yield the Euler equations. Further simplification, by removing terms describing vorticity yields the full potential equations. Finally, these equations can be linearized to yield the linearized potential equations. And this yield equation presents the solution to the problem with defining the appropriate boundary conditions.

Chapter 2

Literature Review

The demand for efficient and cost effective ED processes in the research and academic institutes as well as in industries is rapidly increasing. In industries different type of ED unit designs are developed at micro scale and nano scale to improve efficiency and cost effectiveness. The different investigations done on electrodialysis unit are given in chapter 1. Most of the research work is going on chemical base and specially membrane processes. some of the research was done upon the design aspects of the ED unit but mostly work done in case of single compartment.

In ED process, the flow of water over the surface of the membranes, plays an important role in overall stack resistance, desalting performance, energy consumption, current efficiency etc. that ultimately determine the capital cost and product water cost.

2.1 Flow Pattern[1]

Three different types of flow systems (or design) inside the ED stacks are employed. These are: (i) parallel flow pattern, (ii) series flow pattern, and (iii) parallel-cum-series flow pattern.

2.1.1 Parallel flow pattern in ED stack

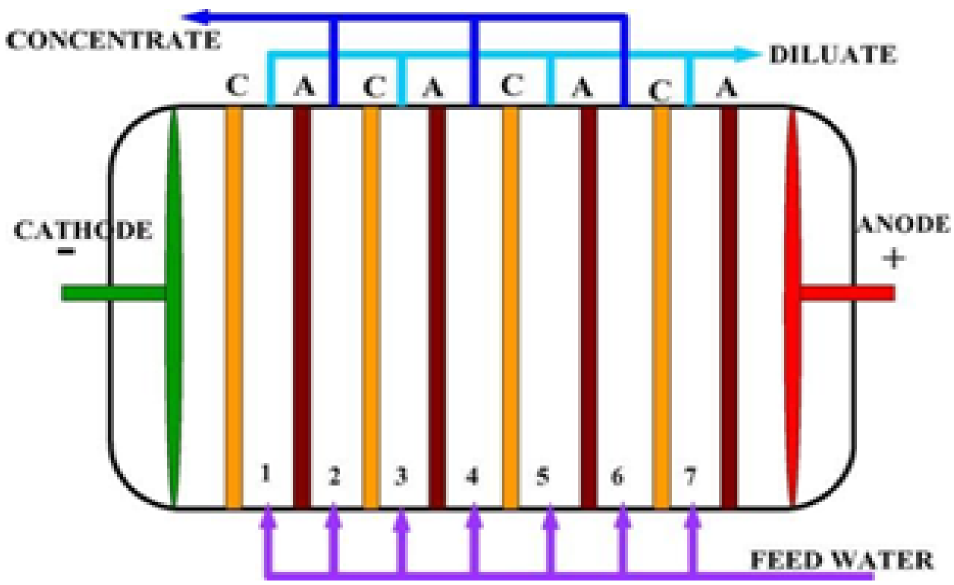

Figure 2.1: Parallel flow pattern in electrodialysis stack

In the parallel flow pattern Fig.2.1, the water stream which has to pass through the dilute and concentrate compartments of the electrodialysis stack is divided at the entry point itself. The individual dilute water inlet stream is fed equally to all the dilute compartments and desalted water is taken out from the other side. Similar thing happens for the concentrate compartments where the outlet streams become rich in salt concentration. Equal stress develop in all the compartments so membranes are safe from high stress. Advantages of parallel flow pattern are:

a. minimum pressure drop

b. equal electrical resistance of each compartment

c. equal desalination in each compartment

d. equal difference of concentration on two sides of membranes

The disadvantages are:

a. uniform flow velocity may not be obtainable in all compartments

b. the flow may choose the path of least resistance which may results to stagnation of water in certain compartments. Continuous desalting of such stagnant water may leads to polarization, which ultimately enhance the resistance of the system.

2.1.2 Series flow pattern in ED stack

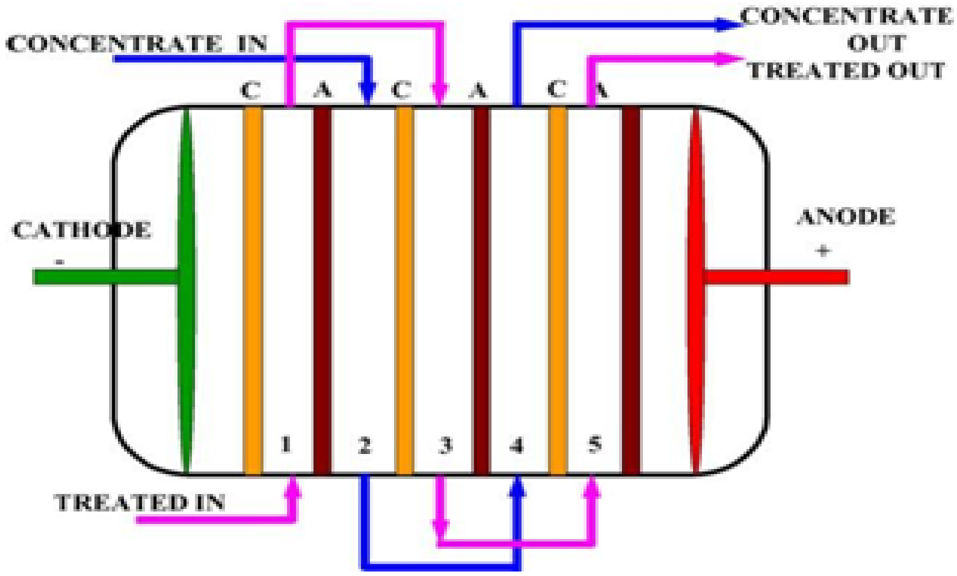

Figure 2.2: series flow pattern in electrodialysis stack.

In series flow pattern, very high linear velocity can be obtained preventing any polarization and thereby leads to high degree of desalting in a single stage. A schematic diagram is given in (Fig.2.2). In this pattern the pressure drop is very high which may cause rupture of membranes if the burst strength value of membrane is exceeded by the difference of pressure on two sides of the membrane. The torque required for making the assembly leak-proof will be very high.

2.1.3 Parallel-cum-series flow pattern in ED stack

To avoid the disadvantages of both the flow patterns and to avail the maximum advantages a combined flow pattern has been introduced, known as parallel-cum-series flow pattern Fig.2.3. Here the degree of desalting can be raised with increase in linear flow velocity.

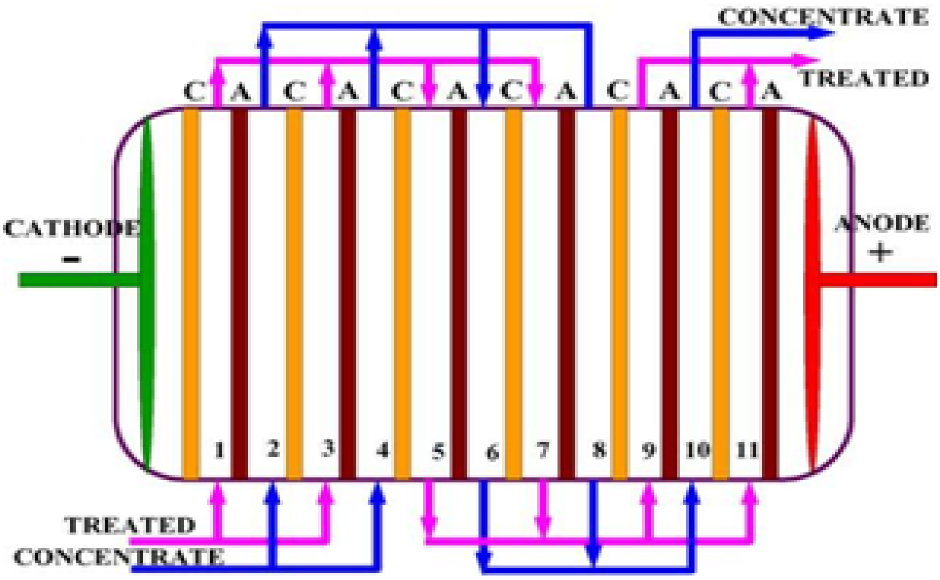

Figure 2.3: Parallel-cum-series flow pattern in electrodialysis stack.

Normally in parallel-cum-series flow pattern equal number of cell pairs is used in each stage, which maintains an equal distribution of flow in all the stages. But by varying the number of cell pairs in each internal stage, the linear velocity in each stage can also be varied as desired. If the number of cell pairs gradually decreases in each stage with the progress of desalting, it results to an increase in linear flow velocity. This type of flow may be defined as a tapered flow pattern.
In this flow pattern, the stack resistance for the same desalting performance is lower than series or parallel-cum-series flow pattern.This type of flow system is advantageous when water of high total dissolved solid (TDS) is to be desalted.

To obtain better desalting performance by an ED stack, a thorough study of resistance developed in each stage by varying the number of stages and also number of cell pairs contained in various stages is necessary. This will enable to design ED stack to improve its performance capability and also increase capacity, which may lead to reduce the capital cost as well as product water cost.
In the present investigation, the flow behavior has been studied for same kind of existing parallel-cum-series type flow pattern ED unit having 3 intermittent stage in series in which no of compartments are arranged in parallel in each stage.

2.2 Water flow analysis using CFD[2]

The water flow inside the treated and rejected compartment and electrode wash in the ED, EDI and CEDI stacks is a complex phenomenon due to parallel, series, parallel and series arrangement of compartments. It becomes more tedious and unpredictable with reference to the transportation of ions from concentrated to treated one. Many investigators [Carl-Ola; 2004] have used computational fluid dynamics to investigate the flow characteristics inside the ED, EDI and CEDI units. The important parameters namely, flow distribution in the compartments, effect of spacer, water distribution through channels, pressure drop, velocity, mass transfer, drag, friction coefficient, etc. were analyzed using the CFD.
Danielsson et. al. (2004)[8]have conducted the flow distribution study for a new Electrodialysis module. They have investigated the flow distribution for three different designs of 4mm thick frames (compartments). The incompressible Navier-Stokes mode of Femlab software was used to solve the averaged Navier-Stokes equations and Darcy flow mode was used for the Thin Film approximation Theory (TFT) equations. Based on the analysis of three frames, better flow distribution frame was manufactured and tested experimentally. They have reported the CFD results are well in the agreement with the experimental results. The efficiency of the unit is determined by the water residence time distribution which depends on the velocity field. A theo-

retical model based on potential flow theory was proposed by Dirkse et al. (2008) for the velocity and pressure filed.Dal-Cin et al. (2006) have predicted the flow and pressure distributions in one bank of a plate and frame ultrafiltration module with five channels in parallel operating in a Z configuration. The prediction were done based on (1) Bernoulli's equation and a momentum balance in one dimension and (2) a three-dimensional field solution (Computational Fluid Dynamics) of the Navier-Stokes equation. CFD solutions were taken as the benchmark and used to refine the 1D model being developed to evaluate flow and pressure distributions for different operating conditions and ultimately different module configurations.Numerical solution of Navier-Stokes equations in a three-dimensional randomly porous packed bed illustrated that the results are in good agreement with those of reported by Macdonald et al. (1979). [A. Jafari. et. al.]. Apart from the CFD analysis, Gimmelshtein and Semiat (2005) have used the particle image velocimetry (PIV) method used for velocity measurements and MI estimations through the spacer between two membranes. The results showed that flow direction changes occur near the spacer mainly due to the existence of an obstacle that the flow had to bypass. They have reported that significant mixing intensity can be found at higher flow rates than those used regularly in membrane processes.
J.L.C. Santos et. al. have experimentally and numerically investigated the flow and mass transfer profiles inside the channels of membrane module. The results were obtained for 12 different flow aligned spacer structures under different hydrodynamics conditions.

Fluid flow devices often employ multiple parallel channels, for example, to enhance heat transfer in heat exchangers, enhance mass transfer in absorbers, or improve fluid transport and distribution in fuel cell gas channels. The smaller channels provide increased surface area, while the inlet and exit manifolds facilitate necessary distribution and provide connections to external inlet and outlet conduits. Flow maldistribution in heat exchangers has been studied by a number of researchers. Non-uniform flow in channels leads to different performance penalties depending on the process. For example, gross flow maldistribution leads to significant reduction in effectiveness for high NTU heat exchangers[9], about 7% for condensers, and up to 25% for cross-flow exchangers[10]. Mueller and Chiou [9] list various factors responsible for flow maldistribution in a shell and tube heat exchanger: entry problems due to header design, bypass streams and fabrication tolerance Kitto and Robertson[11] provide a good summary of maldistribution in heat exchangers and indicate that the problem is more severe in two-phase devices, such as evaporators, condensers, absorbers, re-boilers, etc.

In general, maldistribution in parallel channels is caused by: (a) Uneven local pressure distribution in the inlet/exit manifolds apparent at the channel entrance/exit, caused by the specific placement of the inlet/outlet pipes, fluid distribution in the headers, buoyancy effects, two-phase separation and resultant flow non-uniformity.

(b) Uneven flow resistances in the parallel channels caused by variations in channel dimensions, different flow lengths, uneven fouling, density and viscosity variations, and presence of two or more phases.

Lalot et al.[10] identified that the kinetic energy of the fluid brought in by the inlet pipe into the inlet manifold causes local pressure variations at the entrance to the channels. The local pressure distribution at the face of the channels is affected by the local velocity distribution. If the inlet pipe is facing the channel entrance, then the pressure in the area immediately facing the pipe has an additional pressure head of $1/2\ \rho\ V^2$ due to the inlet velocity V. The local velocity vectors at the entrance to each channel determine this additional head, which could result in a reverse flow in the channels under extreme conditions.

Plate heat exchangers have been investigated extensively for the pressure variations in the inlet ports and its implication in flow maldistribution and performance degradation. Tereda et al.[12] measured the pressure distribution inside the port and individual channels of a plate heat exchanger to estimate the flow rates in different channels without disturbing the flow.Bobbill et al.[13] developed a generalized mathematical model to study the effect of flow maldistribution on the condensation in a plate heat exchanger.Bobbill et al.[14] measured the port to channel pressure drop by introducing pressure probes. Their results indicate that the flow maldistribution increases with increase in the overall pressure drop. Li et al.[15] used the particle image velocimetry (PIV) technique to investigate the flow characteristics of the flow field in the entrance region of a plate-fin heat exchanger. Rao et al.[16] conducted experimental and theoretical study to show that the performance of a heat exchanger was affected by the port-to-channel flow maldistribution in single-pass and multipass heat exchangers. The maldistribution reduced with multi passing. The effect of the manifold was investigated analytically by Baek and Jiao[17]. They found that optimizing the distributor configuration greatly reduced the flow maldistribution. Rao and Das[18] confirmed the validity of their analytical techniques that showed that the pressure drop increases with the presence of flow maldistribution in a plate heat exchanger. Zhang et al.[19] and Jiao et al.[20][21] experimentally studied the flow maldistribution caused by the defects in the inlet configuration and emphasized the need for proper distributor design.

A uniform distribution of current density is of paramount importance for fuel cell operation; it leads to uniform distribution of temperature and liquid water production, and lower mechanical stresses on the membrane electrode assembly (MEA)[22]. The current density distribution in a PEMFC is determined by the uniformity of the reactant gas supply over the catalyst layer. Flow maldistribution is also an important factor in reducing the operating life of a fuel cell[23][24]. Proper reactant distribution is therefore critical to ensure high performance and long lifetime of a PEMFC.

Flow field design and header configuration significantly affect the flow non-uniformity. Various complex flow fields, such as serpentine channels, multiple parallel channels and interdigitated channels, have been investigated for flow maldistribution in PEM fuel cells. Dutta et al.[25][26] examined the performance of straight and serpentine channels. Jen et al.[27] predicted the cell performance with straight channels. A.Kumar and Reddy[28] examined the impact of channel dimensions and shape for serpentine flow fields on cell performance and later for porous metal foams[29]. They observed a more uniform current density distribution with metal foam compared to a multi-parallel channel flow field design. Senn and Poulikakos[30] and Hontanon et al.[31] also found that porous materials yielded better flow distributions and improved mass transfer, and consequently higher cell performance compared to grooved straight and serpentine flow channels. Barreras et al.[32][33] implemented flow visualization by the laser-induced fluorescence as well as measurements of the velocity field by dye trace tracking to study the flow distribution in a parallel diagonal channel, a branching cascade type, and a serpentine-parallel flow topology. They found that very homogeneous velocity and pressure fields are obtained for both the serpentine-parallel and the cascade type flow topologies, while an uneven flow distribution was obtained with the diagonal topology. Um and Wang[34] and Hu et al.[35] compared the interdigitated flow channels with parallel straight channels and reported that an interdigitated flow channel could enhance mass transport and improve the PEMFC performance compared to a parallel channel due to forced convectional flow through the porous diffusion layer. Birgersson and Vynnycky[36] numerically simulated and quantitatively compared the performance of the interdigitated channels, parallel channels, and porous foam, and concluded that the foam yielded the most uniform current density distribution and the interdigitated channels consisting the highest current densities. The advantage and disadvantage of some of the flow-fields have been discussed in several reviews[37][38].

At the stack level, flow maldistribution is more severe due to the multi-duct (individual cells are sometimes referred to as ducts) configuration. However, due to the complexity of the problem and the lack of an experimental technique to measure the instantaneous flow distribution, very few investigations have been reported for the stack level maldistribution. Ganesh et al.[39] mathematically defined a flow maldistribution parameter in terms of the duct inlet velocity and numerically simulated the flow distribution in a PEMFC stack by using flow channeling theory and found a considerably skewed flow distribution which is dominated by flow rate and port size. Bansode et al.[40] carried out a 3D numerical single-phase study to analyze the flow maldistribution in a PEMFC stack with four ducts. Their results showed that the variation in port diameter leads to different degrees of maldistribution and the corresponding non-uniform water content in the membrane. Koh et al.[41] reported a numerical model to investigate pressure variation and flow distribution of stacks. Chen et al.[42] constructed a 2D stack model composed of 72 cells filled with a porous medium to evaluate pressure variation and flow distribution in the manifold of a fuel cell stack. Their modeling results indicated that although both the channel resistance and the manifold width can enhance the uniformity of the flow distribution, larger manifold width is a better solution for flow distribution because increasing the channel resistance requires an excessive pressure drop which is not beneficial in practical applications.

Similar to the results obtained for heat exchangers[12], the flow maldistribution is induced not only by the cell design but also by local water blockage in the channels. Water accumulation (resulting from vapor condensation and/or product water) in the catalyst layer, GDL, and in gas channels will fill the pores from micro- to macro-sizes and block the gas pathways. This is the well-known flooding phenomenon which can cause major problems with gas distribution and consequently damage the cathode catalyst layers[43]. Presence of water in the individual channels leads to different two-phase flow patterns that affect the gas flow rates in those channels as well as in the other parallel channels due to cross-communication between the channels through the manifolds. An important objective of this work is to identify the flow maldistribution caused by the presence of water in the channels and investigate the flow interaction between adjacent channels.

Flow distribution studies in PEMFCs were primarily limited to flow fields without considering the effect of the gas diffusion layer. In a PEMFC the flow fields are in direct contact with the diffusion layer which helps in distributing the reactants uniformly over the catalyst layer. Consequently, the flow distribution in the flow field needs to be further linked with the flow distribution in the diffusion layer. Dole et al.[44] studied the interaction between the diffusion layer with different permeability and flow field designs, and concluded that even a meander structure distributes the reactants non-homogeneously on the electrodes due to the additional flow paths available in the diffusion layer. Kanezaki et al.[45] studied the cross-leakage flow between adjacent flow channels in a single channel serpentine flow field and found a significant amount of the cross-leakage flow. This flow is comparable with the flow in the serpentine path due to the pressure gradient set up across the porous diffusion layer between the adjacent channels. Given the considerable influence of the diffusion layer on the flow distribution in PEMFC channels, it becomes relevant to measure the instantaneous flow rate in the channels with a diffusion layer backing rather than in channels with impermeable walls.

This report is organized as follows: In the first part, study of flow behavior by visualization technique using die penetration method in lab scale model of actual parallel-cum-series flow pattern of ED unit and single compartment of existing and proposed design. In the second part, CFD analysis of actual scale parallel-cum-series model and single compartment as discussed in first part. And in third part, analysis of both the results carried out.

2.3 Objectives of the study

ED stack is close and leakage proof system and as due to its housing it is not possible to study the flow behavior of stack and its compartment by any visualizing technique. In parallel arrangement of compartments in each stage, uneven distribution of solution inside the compartments occur due to that solution become stagnant in some of the compartments that ultimately lowers the efficiency of the ED stack. So to improve the efficiency solution should be pass by equal quantity of water through each compartment.

When the flow of solution passing through ED stack that gives individual flow for each compartment that are arranged in parallel in each stage. ED stack is close system so it is very difficult to measure the pressure and velocity for each and every compartment experimentally.

CFD analysis is very helpful to study the flow behavior for different compartments and ED stack.To improve ion-exchange some of the design aspects should be investigated for maximum use of membrane area in Existing design of the compartment openings.

2.4 Structure of Thesis

In the present work, flow behavior of ED stack for treated compartment are investigated using CFD analysis and some new design aspect of ED stack would applied and increasing the efficiency of ED unit . Chapter 1

a. chapter 1 of this thesis presents the working principle and importance of elecrodialysis and application of CFD in present work.

b. Chapter 2 summarizes the literature available on the ED stack in reference to the present work and requirement of CFD in development of work that done in literature.

c. Chapter 3 gives overview about CFD and its concept, techniques and ability to solve the complex problems.

d. Chapter 4 presents the experimental set-up and program .

e. Chapter 7 presents modeling and analysis of ED stack and compartments using CFD software.

f. Chapter 6 Presents the detail discussion on the results of the experimental and analysis using CFD and its validation.

g. Chapter 7 summarizes overall conclusions that have been drawn from the present work. In this chapter, the scope of future work is also proposed.

Chapter 3

Computational Fluid Dynamics

3.1 Needs of CFD

The development of the high speed computer and the evolution of the computational fluid dynamics (CFD) have a great influence on the engineering design and analysis of the turbo machinery. In the past decades, due to increasing capability to solve complex geometry and complex flow problems and reduction in computational time and costs, the CFD methodology has emerged to become an efficient approach for collecting information to improve engineering design of turbo machinery. Today, CFD is an equal partner with pure theory and pure experiment in the analysis and solution of fluid dynamics problem, as sketched in Fig.3.1[46]. And CFD will continue to play this role indefinitely, for as long as our advanced human civilization exists.

Compared to theoretical approach to solve fluid flow problems, the CFD approach has the advantage that it can provide a solution for a much more complex problem. And compared to experimental approach, in which cost is proportional to the number of data points and the number of configurations tested, in terms of facility hire and/or man-hour costs, CFD approach can produce extremely large volumes of results at virtually no added expense and it is very cheap to perform parametric studies, for

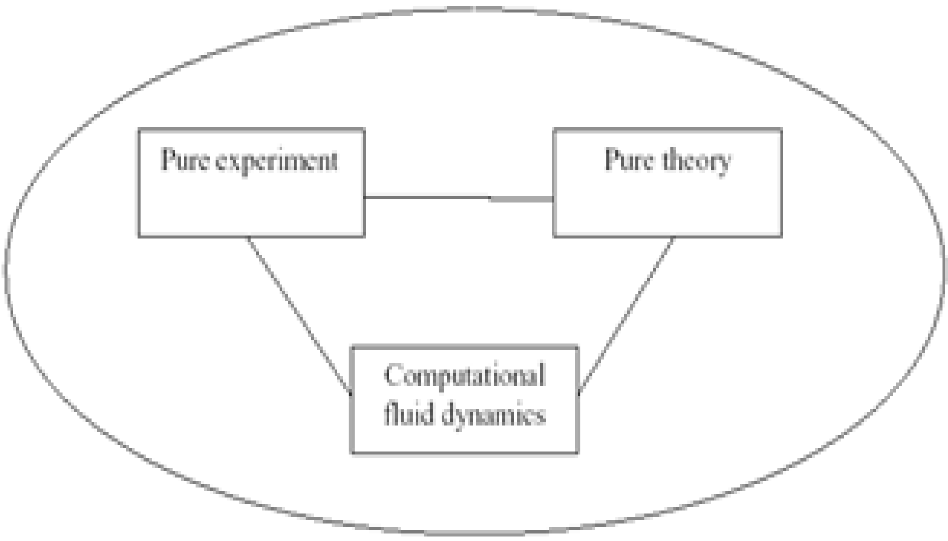

Figure 3.1: The "three dimensions" of fluid dynamics

instance to optimize equipment performance.

However, to keep things in perspective, CFD provides a new third approach- but nothing more than that. It nicely and synergistically complements the other two approaches of pure theory and pure experiment, but it will never replace either of these approaches. There will always be a need for theory and experiment. Rather, the future advancement of fluid dynamics will rest upon a proper balance of all the three approaches, with computational fluid dynamics helping to interpret and understand the results of theory and experiment, and vice versa

3.2 Concept of CFD

The physical aspect of any fluid flow is governed by three conservation laws:

a. Conservation of Mass: The mass of a fluid is conserved.

b. Conservation of Momentum: The rate of change of momentum is equal to the sum of the forces on a fluid particle, in the same direction (Newton's second law).

c. Conservation of Energy: The rate of change of energy is equal to the sum of the rate of heat addition and the rate of work done on a fluid particle (first law of thermodynamics).

These fundamental conservation laws can be expressed in terms of basic mathematical equations, which in their most general form are either integral equations or partial differential equations. Computational fluid dynamics is the art of replacing the integrals or the partial derivatives (as the case may be) in these three fundamental equations with discretized algebraic forms, which in turn are solved to obtain numbers for the flow field values at discrete points in time and/or space. The end product of CFD is indeed a collection of numbers, in contrast to a closed-form analytical solution. However, in the long run, the objective of most engineering analyses, closed form or otherwise, is a quantitative description of the problem, i.e., numbers. Of course, the instrument which has allowed the practical growth of CFD is the high-speed digital computer. CFD solutions generally require the repetitive manipulation of many thousands, even millions, of numbers, a task that is humanly impossible without the aid of a computer. Therefore, advances in CFD, and its applications to problems of more and more detail and sophistication, are intimately related to advances in computer hardware, particularly in regard to storage and execution speed. This is why the strongest force driving the development of new supercomputers is coming from the CFD community. Indeed, the advancement in large mainframe computers has been phenomenal over the past three decades.[47] Thus, in simple words CFD can be defined as:
"CFD is the analysis of systems involving fluid flow, heat transfer and associated phenomena such as chemical reactions by means of computer-based simulation."
The technique is very powerful and spans a wide range of industrial and non-industrial application areas. Some examples are:[47]

a. Aerodynamics of aircraft and vehicles: lift and drag

b. Turbo machinery: flows inside rotating passages, diffusers etc.

c. Hydrodynamics of ships

d. Marine engineering: loads on off-shore structures

e. Biomedical engineering: blood flows through arteries and veins

f. Power plant: combustion in IC engines and gas turbines

g. Chemical process engineering: mixing and separation, polymer moulding

h. Electrical and electronic engineering: cooling of equipment including micro-circuits

i. External and internal environment of buildings: wind loading and heating/ ventilation

j. Environmental engineering: distribution of pollutants and effluents

k. Hydrology and oceanography: flows in rivers, estuaries, oceans

l. Meteorology: weather prediction

The advantages of CFD over experimental approach to fluid system design can be summarized as:

a. Substantial reduction of lead times and costs of new designs.

b. Ability to study systems where controlled experiments are difficult or impossible to perform (e.g. very large systems).

c. Ability to study systems under hazardous conditions at and beyond their normal performance limits (e.g. safety studies and accident scenarios).

d. Practically unlimited level of detail of results.[47]

3.3 Steps To Solve The Problem Using CFD Approach

The various steps required to solve the problem using CFD are described below.[48]

3.3.1 Creation of Mathematical Model

The starting point of any numerical method is to convert the physical problem into the mathematical model, i.e. the set of partial differential or integral-differential equations and specify the boundary conditions. One chooses an appropriate model for the target application (incompressible, inviscid, turbulent; two- or three-dimensional, etc.). As already mentioned, this model may include simplifications of the exact conservation laws. A solution method is usually designed for a particular set of equations. Trying to produce a general purpose solution method, i.e. one which is applicable to all flows, is impractical, if not impossible and, as with most general purpose tools, they are usually not optimum for any one application.

3.3.2 Choose a Discretization Method

After selecting the mathematical model, one has to choose a suitable discretization method (Section 3.5), i.e. a method of approximating the differential/integral equations by a system of algebraic equations for the variables at some set of discrete locations in space and time. There are many methods, but the most important ones are:

a. Finite Difference Method (FDM)

b. Finite Volume Method (FVM) and

c. Finite Element Method (FEM)

Other methods, like spectral schemes, boundary element methods, and cellular automata are used in CFD but their use is limited to special classes of problems. Each type of method yields the same solution if the grid is very fine. However, some methods are more suitable to some classes of problems than others. The preference is often determined by the attitude of the developer.

3.3.3 Numerical Grid Generation

The discrete locations at which the variables are to be calculated are defined by the numerical grid which is essentially a discrete representation of the geometric domain on which the problem is to be solved. It divides the solution domain into a finite number of sub domains (elements, control volumes etc.) and gives the set of discrete points for the discretization scheme. Some of the options available are the following:

Structured (regular) Grid

Regular or structured grids consist of families of grid lines with the property that members of a single family do not cross each other and cross each member of the other families only once. An example of a structured 2D grid is shown in Fig.3.2,designed for calculations of flow in a symmerty segment of a staggered tube bank.[48]

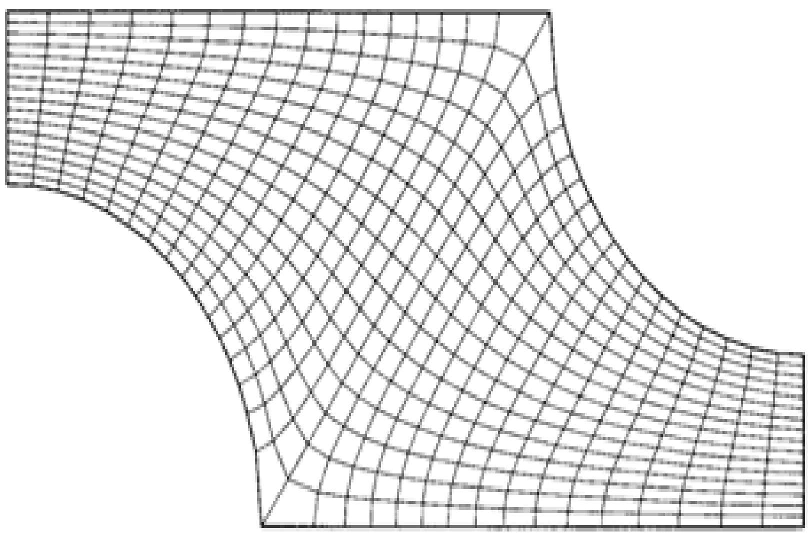

Figure 3.2: Example of a 2D, structured, non-orthogonal grid

Unstructured grids

For very complex geometries, the most flexible type of grid is one which can fit an arbitrary solution domain boundary. In principle, such grids could be used with any discretization scheme, but they are best adapted to the finite volume and finite element approaches. In practice, grids made of triangles or quadrilaterals in 2D, and tetrahedra or hexahedra in 3D are most often used.
An example of an unstructured grid[48] is shown in Fig.3.3

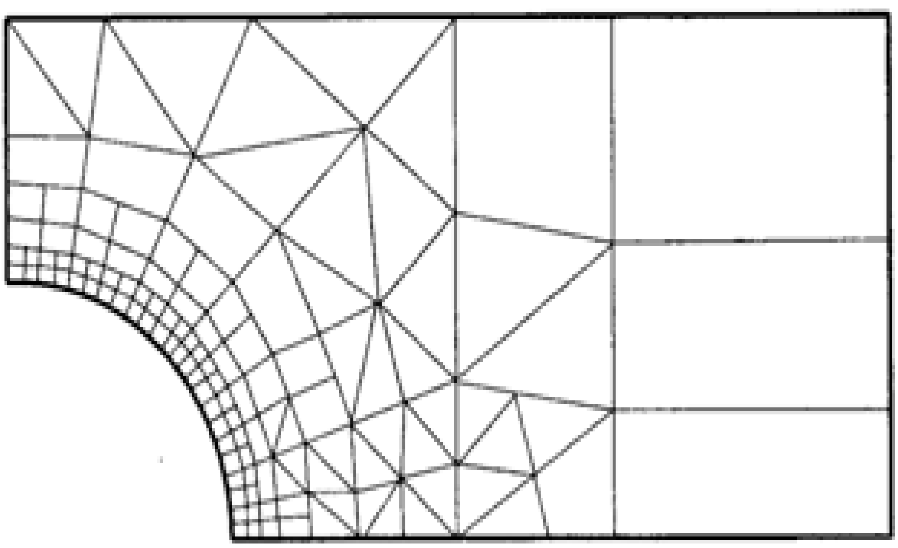

Figure 3.3: Example of a 2D unstructured grid

3.3.4 Finite Approximation

After selecting the type of grid, the next step is the finite approximations to be used in the discretization process. In a finite difference method, approximations for the derivatives at the grid points have to be selected. In a finite volume method, one has to select the methods of approximating surface and volume integrals. In a finite element method, one has to choose the shape functions (elements) and weighting functions.

3.3.5 Solution of Algebraic Equations

Discretization yields a large system of algebraic equations. The method of solution of these algebraic equations depends on the type of the problem i.e. steady or unsteady. For unsteady flows, methods based on those used for initial value problems for ordinary differential equations (marching in time) are used. Steady flow problems are usually solved by pseudo-time marching or an equivalent iteration scheme. The choice of solver depends on the grid type and the number of nodes involved in each algebraic equation.

3.3.6 Convergence Criteria

Finally, one needs to set the convergence criteria for the iterative method. Usually, there are two levels of iterations: inner iterations, within which the linear equation are solved, and outer iterations, that deal with the non-linearity and coupling of the equations. Deciding when to stop the iterative process on each level is important, from both the accuracy and efficiency points of view.

3.4 Discretization Methods

Basically two types of problems are there in fluid flow e.g. steady state and unsteady state. The equations of steady flow are independent of time, thus the model equation contain partial derivatives with respect to space only. But equations governing unsteady fluid flow are time dependent, thus the model equations contain partial derivatives with respect to both space and time. We can approximate these equations simultaneously and solve the resulting difference equations. The approximation can be done by any one of the following methods.

3.4.1 Finite Difference Method (FDM)

The first step in obtaining a numerical solution is to discretize the geometric domain i.e. a numerical grid must be defined. In finite difference method (FDM) discretization methods the grid is usually locally structured, i.e. each grid node may be considered the origin of a local coordinate system, whose axes coincide with grid lines. This also implies that two grid lines belonging to the same family, say xi_1, do not intersect, and that any pair of grid lines belonging to different families, say ξ_1 = const, and xi_2 = const., intersect only once. In three dimensions, three grid lines intersect at each node; none of these lines intersect each other at any other point. Fig.3.4shows examples of one-dimensional (1D) and two-dimensional (2D) Cartesian grids used in FDM.

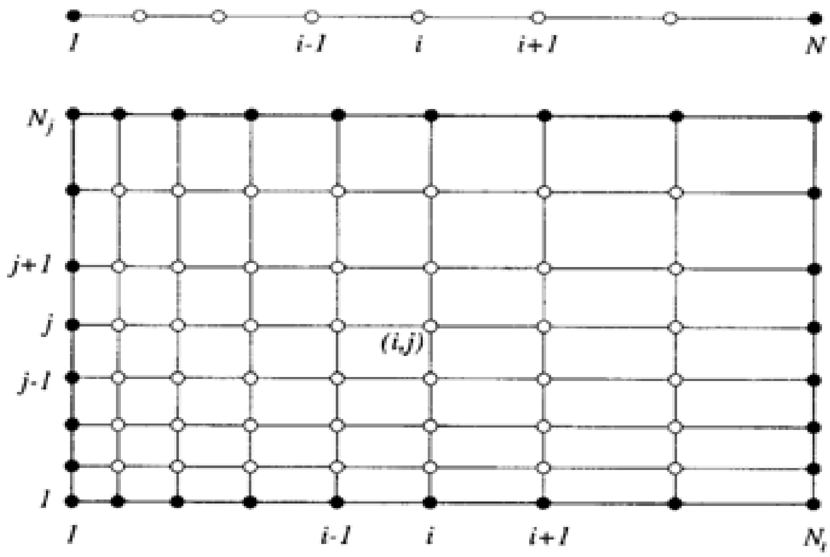

Figure 3.4: 1D (above) and 2D (below) cartesian grid for FDM

Each node is uniquely identified by a set of indices, which are the indices of the grid lines that intersect at it, (i, j) in 2D and (i, j, k) in 3D. The neighbor nodes are defined by increasing or reducing one of the indices by unity.

D(ϕ) = k where, D is differential operator k is source term ϕ is parameter
In FDM the whole domain is divided into a large number of smaller elements which depends on accuracy of the solution required and derivatives are replaced by finite difference approximation.Similarly for higher derivatives we have finite difference approximations.
The idea behind finite difference approximations is borrowed directly from the definition of a derivative:

$$(\frac{\partial\phi}{\partial x})_{xi} = \lim \frac{\phi(x_i + \triangle x) - \phi(x_i)}{\triangle x} \tag{3.1}$$

These approximations give system of algebraic equations which are then solved using computer. This is the simplest of all available approximations and easy to calculate.FDM is usually used for structured grid.[48]

3.4.2 Finite Volume Method (FVM)

Finite-volume methods have become popular in CFD as a result, primarily, of two advantages. First, they ensure that the discretization is conservative, i.e., mass, momentum, and energy are conserved in a discrete sense. While this property can usually be obtained using a finite-difference formulation, it is obtained naturally from a finite-volume formulation. Second, finite volume methods do not require a coordinate transformation in order to be applied on irregular meshes. As a result, they can be applied on unstructured meshes consisting of arbitrary polyhedra in three dimensions or arbitrary polygons in two dimensions. In FVM, the problem domain is divided into large number of small (finite) volumes. Integral forms of conservative equations are applied to each control volume. Conservation principles obey over each control volume and as well as to the entire domain. This leads to system of algebraic equations obtained for each control volume by suing appropriate approximate quadrature schemes, and these equations are then solved using computer. Fig.3.5shows a typical CV and the notation used for a cartesian 2D grid in FVM.

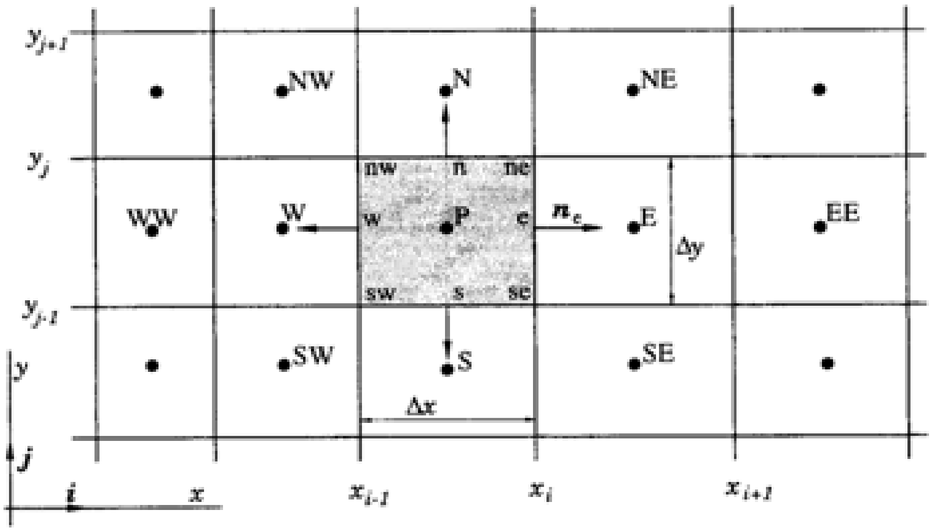

Figure 3.5: A typical control volume and the notation used for a cartesian 2D grid in FVM

3.4.3 Finite Element Method (FEM)

This method was basically originated in the study of structural mechanics problems. It is most popular in structural mechanics and solid mechanics related fields. In general, finite element method (FEM) is versatile in applications to multidimensional complex irregular geometries. In this method, problem domain is divided into small elements called finite elements. Using appropriate interpolation functions, approximation of function in terms of nodal values is carried out. Substitution of these approximations into governing equation (integral and differential equations) leads to system of algebraic equations, which are then solved using computer.

3.4.4 Mathematical Model[3]

CFD is a numerical technique to obtain an approximate solution numerically[3]. We have to use a discretization method, which approximate the differential equations by

a system of algebraic equations, which can then be solved on a computer. The approximations are applied to small domain in space and/or time so that the numerical solution provides results at discrete locations in space and/or time.
The physical aspect of any fluid flow is governed by the following three fundamental principles:

a. Conservation of Mass

b. Conservation of Momentum

c. Conservation of Energy

These fundamental principles can be expressed in terms of partial differential equations. CFD is a numerical technique to replace these partial differential equations of fluid flow into the algebraic equations by numbers and discretizing them in space and/or time domain. With the advent of high speed digital computers, CFD has become a powerful tool to predict flow characteristics in various problems in an economical way.

Conservation Equations

Mass conservation equation

The equation for conservation of mass, or continuity equation, can be written as follows:

$$\frac{\partial \rho}{\partial t} + \nabla.(\rho V) = S_m \tag{3.2}$$

This equation is the general form of the mass conservation equation and is valid for incompressible as well as compressible flows. The source S_m is the mass added to the continuous phase from the dispersed second phase (e.g., due to vaporization of liquid droplets) and any user-defined sources. **Momentum conservation equation**
Conservation of momentum in an inertial (non-accelerating) reference frame is de-

scribed by

$$\frac{\partial}{\partial t}(\rho v) + \nabla(\rho v v) = -\partial p + \partial(\tau) + \rho g + F \tag{3.3}$$

where,

p is the static pressure, τ is the stress tensor (described below), and ρg and F are the gravitational body force and external body forces (e.g., that arise from interaction with the dispersed phase), respectively. F also contains other model-dependent source terms such as porous-media and user-defined sources.

The stress tensor τ is given by,

$$\tau = \mu[(\nabla V + \nabla V^T) - 2/3\nabla.V.I] \tag{3.4}$$

where, μ is the molecular viscosity I is the unit tensor, and the second term on the right hand side is the effect of volume dilation.

3.4.5 Discretization

A control-volume-based technique is used to convert the governing equations to algebraic equations that can be solved numerically. This control volume technique consists of integrating the governing equations about each control volume, yielding discrete equations that conserve each quantity on a control-volume basis.Discretization of the governing equations can be illustrated most easily by considering the steady-state conservation equation for transport of a scalar quantity ϕ over control volume V as follows.

$$\oint \rho\phi V.dA = \oint \Gamma_\phi \nabla_\phi dA + \int_v S_\phi dV \tag{3.5}$$

where, ρ is density, v is velocity vector, dA is surface area vector, Γ_ϕ is diffusion coefficient for ϕ, V_ϕ is gradient of ϕ and S_ϕ is source of ϕ per unit volume

Above equation is applied to each control volume, or cell, in the computational domain. Discretization of the equation on a given cell yields,

$$\Sigma\rho_f\phi_f V_f A_f = \Sigma\Gamma_\phi(\nabla_\phi)_n A_f + S_\phi V \tag{3.6}$$

where, ϕ_f is value of ϕ convected through face f ρ_f . V_f . A_f shows mass flux through the face A_f is area of face f $(V_\phi)_n$ is magnitude of V_ϕ normal to face f V is cell volume The equations solved by FLUENT take the same general form as the one given above and apply readily to multi-dimensional, unstructured meshes composed of arbitrary polyhedra. By default, FLUENT stores discrete values of the scalar ϕ at the cell centers. However, face values ϕ_f is required for the convection terms in equation 3.15 and must be interpolated from the cell center values. This is accomplished using an upwind scheme.

Upwinding means that the face value ϕ_f is derived from quantities in the cell upstream, or "upwind," relative to the direction of the normal velocity V_n in equation. FLUENT allows us to choose from several upwind schemes: first-order upwind, second-order upwind, power law, and QUICK. The diffusion terms in equations are central-differenced and are always second order accurate.

Under-relaxation

Because of the nonlinearity of the equation set being solved by FLUENT, it is necessary to control the change of ϕ. This is typically achieved by under-relaxation, which reduces the change of ϕ produced during each iteration. In a simple form, the new value of the variable ϕ within a cell depends upon the old value, ϕ_{old}, the computed change in ϕ, $\Delta\phi$, and the under-relaxation factor, α, as follows:

$$\phi = \phi_{old} + \alpha\Delta_\phi \tag{3.7}$$

For most flows, the default under-relaxation factors do not usually require modification. If unstable or divergent behavior is observed, however, it is required to reduce the under-relaxation factors for pressure, momentum, k, and ϵ from their default values of 0.5, 0.7, 0.8 and 0.8 to about 0.2, 0.5, 0.5 and 0.5 respectively.

Discretization of the continuity equation

The steady-state continuity equation in integral form is given by:

$$\oint \rho v dA = 0 \tag{3.8}$$

This equation may be integrated over the control volume to yield the following discrete equation:

$$\Sigma J_f A_f = 0 \tag{3.9}$$

where, J_f is the mass flux through face f,ρ v_n.
The face value of velocity is not averaged linearly; instead, momentum-weighted averaging, using weighting factors, which can be written as:

$$J_f = J_f + d_f(p_{co} P_{c1}) \tag{3.10}$$

where, p_{c0} and p_{c1} are the pressures within the two cells on either side of the face, and J_f contains the influence of velocities in these cells.
The term d_f is a function of a_P, the average of the momentum equation a_P coefficients for the cells on either side of face f.

Discretization of the momentum equation

The discretized x-momentum equation is:

$$a_p u = \Sigma a_{nb} u_{nb} + \Sigma p_f A.i = S \tag{3.11}$$

The pressure field and face mass fluxes are not known a priori and must be obtained as a part of the solution.FLUENT uses a co-located scheme, whereby pressure and velocity are both stored at cell centers. However, above equation requires the value of the pressure at the face between cells. Therefore, an interpolation scheme is required to compute the face values of pressure from the cell values.

Convergence Criteria

At the end of each solver iteration, the residual sum for each of the conserved variables is computed. On a computer with infinite precision, these residuals will go to zero as the solution converges. On an actual computer, the residuals decay to some small value ("round-off") and then stop changing ("level out"). For "single precision" computations, residuals can drop as many as six orders of magnitude before hitting round-off whereas double precision residuals can drop up to twelve orders of magnitude. Hence, double precision solver gives more accurate results that single precision but it requires more computational time and memory.
After discretization, the conservation equation for a general variable ϕ at a cell P can be written as,

$$a_p \phi_p = \Sigma a_{nb} \phi_{nb} + b \tag{3.12}$$

Here,a_p is the center coefficient, a_{nb} are the influence coefficients for the neighboring cells, and b is the contribution of the constant part of the source term Sc in $S_c = S_c + S_{P*\phi}$ and of the boundary conditions. In equation shown below,

$$a_p = \Sigma a_{nb} - S_p \tag{3.13}$$

The residual R^{ϕ} computed by FLUENT's segregated solver is the imbalance in equation below, summed over all the computational cells P. This is referred to as the "unscaled" residual. It may be written as

$$R^{\phi} = \Sigma \| \Sigma a_{nb} \phi_{nb} + b - a_p \phi_p \| \tag{3.14}$$

In general, it is difficult to judge convergence by examining the residuals defined by equation 3.23 since no scaling is employed. FLUENT scales the residual using a scaling factor representative of the flow rate of ϕ through the domain. This "scaled" residual is defined as

$$R^{\phi} = \frac{\Sigma_P |\Sigma_{nb} a_{nb} \phi_{nb} + b - a_p \phi_p|}{|a_p \phi_p|} \tag{3.15}$$

For the momentum equations the denominator term $a_P \ \phi_P$ is replaced by $a_P \ v_P$, where v_P is the magnitude of the velocity at cell P.
For the continuity equation, the unscaled residual is defined as

$$R^c = \sum |rateofmasscreationincellP| \tag{3.16}$$

And, scaled residual for the continuity equation is defined as

$$\frac{(R)_{iterationN}}{R_{iteration5}} \tag{3.17}$$

The denominator is the largest absolute value of the continuity residual in the first five iterations. Sometimes the residuals may not fall below the convergence criterion set in the case setup. However, monitoring the representative flow variables through iterations may show that the residuals have stagnated and do not change with further iterations. This could also be considered as convergence. (FLUENT 6.1- Tutorial Guide) In the present work, these scaled residuals have been continuously monitored and iteration continued till the limiting value prescribed. It has been observed that, with this default convergence criterion, simulated solution is reasonably accurate. However, in case of the complicated geometry, this default criterion can be further reduced to get a better solution.

Examine the Mesh

It is very important to check the quality of the resulting mesh, because properties such as skewness can greatly affect the accuracy and robustness of the CFD solution. The skewness is classified in two ways, EquiAngle skew and EquiSize skew. Their value ranges from 0 to 1, and lower value is desirable. It is also important to verify that all the elements have positive area/volume, otherwise simulation is not possible. The brief description of EquiAngle skew and EquiSize skew are as follow:

a. **EquiAngle skew** The EquiAngle Skew (QEAS) is a normalized measure of skewness that is defined as:

$$Q_{EAS} = \frac{\theta_{max} - \theta_{eq}}{180 - \theta_{eq}}, \frac{\theta_{eq} - \theta_{min}}{\theta_{eq}} \tag{3.18}$$

where, θ_{max} and θ_{min} are maximum and minimum angles (in degrees) between the edges of the element, θ_{eq} is characteristic angle corresponding to an equilateral cell of similar form for triangular and tetrahedral elements,
$\Theta_{eq} = 60$
For quadrilateral and hexahedral elements,
$\Theta_{eq} = 90$
By definition,
$0 \leqslant Q_{EAS} \leqslant 1$
where, $Q_{EAS} = 0$, describes an equilateral element, and $Q_{EAS} = 1$, describes a completely degenerate (poorly shaped) element.
In general, high-quality meshes contain elements that possess average Q_{EAS} values of 0.1 in 2-Dimensional cases and 0.4 in 3-Dimensional cases.

b. **EquiSize skew** The EquiSize Skew (Q_{EVS}) is a measure of skewness that is defined as:

$$Q_{EVS} = \frac{S_{eq} - S}{S_{eq}} \tag{3.19}$$

where, S is area (2-D) or volume (3-D) of the mesh element Seq is maximum area (2-D) or volume (3-D) of an equilateral cell the circumscribing radius of which is identical to that of the mesh element By definition, $0 \leqslant Q_{EVS} \leqslant 1$ where, $Q_{EVS} = 0$, describes an equilateral element, and $Q_{EVS} = 1$, describes a completely degenerate (poorly shaped) element
In general, high-quality meshes contain elements that possess average Q_{EVS} values of 0.1 in 2-Dimensional cases and 0.4 in 3-Dimensional cases.

3.5 Theoretical Flow Field Studies For Thin Plate

The flow field through the cell has to be calculated using CFD software. Rather than solving a full 3-D problem for the whole module a simplified 2D model was applied which could be solved using Gambit/Fluent, with less computational effort.

3.5.1 Governing Equations

The governing equations for the velocity field, u = (u,v,w), and the pressure, P, are the equations for continuity of mass and momentum. Navier-Stokes equations.

3.5.2 Governing Equation

$$\rho(\frac{\partial u}{\partial t}) + u.\nabla u = -\nabla p + \mu \nabla^2 u \frac{\partial u}{\partial t} + \nabla \rho u = 0 \tag{3.20}$$

In Fig.3.6 the three different regions namely, the inlet region, the active area and the outlet region are shown. The inlet region distributes the flow and provides a uniform

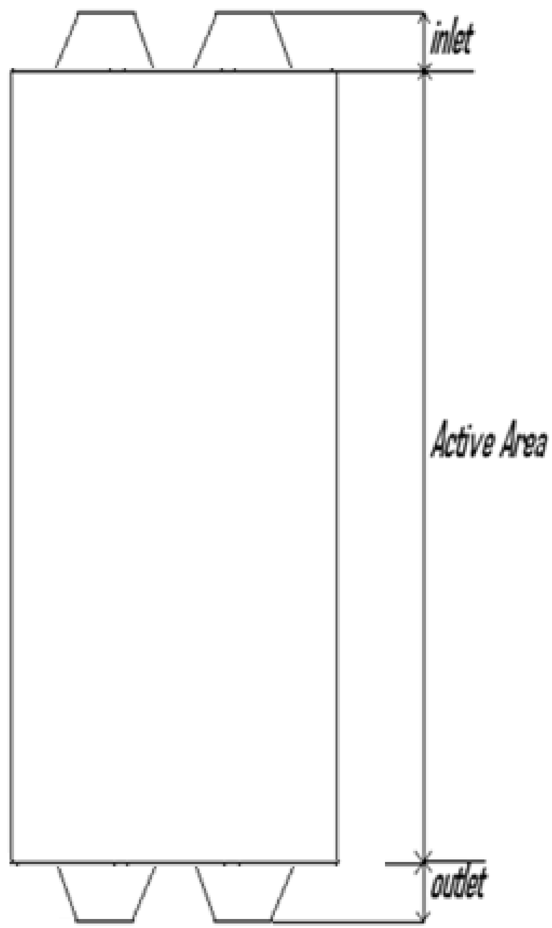

Figure 3.6: Compartment with different flow regions [Carl-Ola et.al.; 2004]

flow distribution before the active area. The active area is where the ionic transport over the membranes takes place in continuous electro deionization module. Finally in the outlet region the fluid is collected into the outlet stream. The length scale used to scale the equations is the length of the active area, L(0.25 m). The height of the flow compartment in the z-direction, perpendicular to the figure, h (0.005) is small so that σ="h/L" is very small. The equations are made non-dimensional by introducing the following variables,

$$\overline{x} = \frac{x}{L}, \overline{y} = \frac{y}{L}, \overline{z} = \frac{z}{L} \overline{u} = \frac{u}{uO}, \overline{v} = \frac{v}{uO}, \overline{w} = \frac{w}{\rho uO}, \overline{p} = \frac{p}{\rho uO^2} \tag{3.21}$$

Where, σ=h/L is a small dimensionless parameter for a long and slender geometry. The length scale L here is the length of the active area and h is half the height of the flow channel. Inserting these non-dimensional variables into the steady state form of the Navier-Stokes equations yields.

$$\overline{u}\frac{\partial\overline{u}}{\partial\overline{x}}+\overline{v}\frac{\partial\overline{u}}{\partial\overline{y}}+\overline{w}\frac{\partial\overline{u}}{\partial\overline{z}}=\frac{\partial\overline{p}}{\partial\overline{x}}+\frac{1}{R_e}(\frac{\partial^2\overline{u}}{\partial\overline{x}^2}+\frac{\partial^2\overline{u}}{\partial\overline{y}^2}+\frac{\partial^2\overline{u}}{\partial\overline{z}^2}) \tag{3.22}$$

$$\overline{u}\frac{\partial\overline{v}}{\partial\overline{x}}+\overline{v}\frac{\partial\overline{v}}{\partial\overline{y}}+\overline{w}\frac{\partial\overline{v}}{\partial\overline{z}}=\frac{\partial\overline{p}}{\partial\overline{y}}+\frac{1}{R_e}(\frac{\partial^2\overline{v}}{\partial\overline{x}^2}+\frac{\partial^2\overline{v}}{\partial\overline{y}^2}+\frac{\partial^2\overline{v}}{\partial\overline{z}^2}) \tag{3.23}$$

$$\overline{u}\frac{\partial\overline{w}}{\partial\overline{x}}+\overline{v}\frac{\partial\overline{w}}{\partial\overline{y}}+\overline{w}\frac{\partial\overline{w}}{\partial\overline{z}}=\frac{\partial\overline{p}}{\partial\overline{z}}+\frac{1}{R_e}(\frac{\partial^2\overline{w}}{\partial\overline{x}^2}+\frac{\partial^2\overline{w}}{\partial\overline{y}^2}+\frac{\partial^2\overline{w}}{\partial\overline{z}^2}) \tag{3.24}$$

Where, Re=ρuL/μ is the Reynolds number. The conservation of mass equation for an incompressible fluid gives,

$$\frac{\partial\overline{u}}{\partial\overline{x}}+\frac{\partial\overline{v}}{\partial\overline{y}}+\frac{\partial\overline{w}}{\partial\overline{z}} \tag{3.25}$$

3.5.3 Two different method of theoretical flow field study for thin plate

The theoretical flow distributions inside compartment is using two method namely as, TFT (thin film flow approximation) and averaged Navier strokes equation.

Thin film flow approximation[49]

The velocity used in the scaling of the equations leading to the thin film approximation, was the linear flow velocity of the liquid in the active area of the module. In the inlet and outlet sections of the cell the velocities of the liquid is about one order of magnitude higher, furthermore the length of these regions is about one order of magnitude lower. Using the thin film approximation in this region might be a bit optimistic. Therefore an alternative formulation of the 2-D momentum balance equations was also considered.

Averaged Navier-Stokes equation[49]

Averaged equations for the flow distribution in the X-Y plane are obtained by integrating the equations for the u and v velocities over the gap between the membranes. The Navier-Stokes equations are integrated over channel height from Z=-h to Z=h

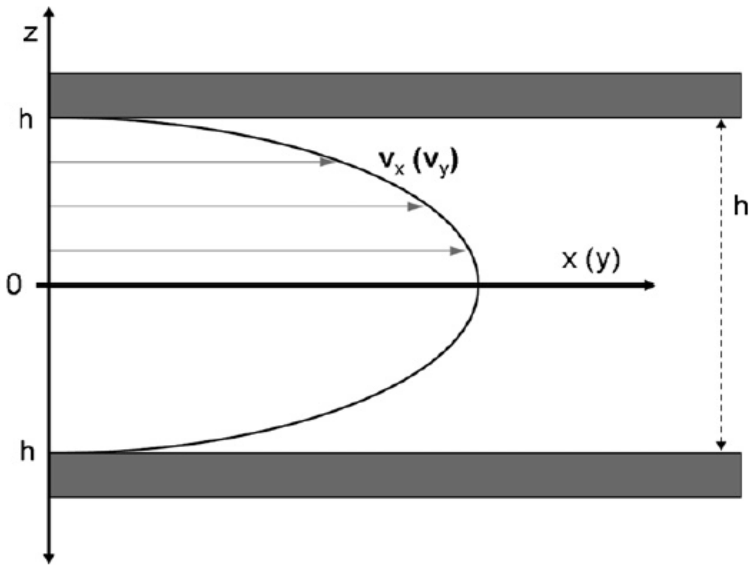

Figure 3.7: Parabolic profile of the vx and vy, components of the velocity vector, h -height of the channel, i.e. distance between plates.

First, an empty channel between two parallel plates with distance h is considered in order to derive a momentum equation of flow in one sub-layer. The channel is perpendicular to the z axis,as shown in Fig. 3. The flow in the channel is characterized by velocity vector v=(vx, vy, vz) being a function of space. When the channel is characterized by low h, the flow inside is fully developed and laminar, then vx and vy are parabolic functions of z, while vz can be neglected, see Fig.3.7.[50].The derivation starts with the fundamental Navier-Stokes equation, see Equation below:

$$\rho \frac{D_v}{D_t} = \eta \Delta^2 V - \Delta P \tag{3.26}$$

where,ρ- fluid density [kg/m^3]; μ- dynamic viscosity [Pa s]; p - pressure [Pa]; t - time [s]; D/Dt - convective derivative.

Since the stationary laminar flow is taken into account, the convective derivative term is neglected. By averaging vx and vy along z using the no-slip boundary condition, the 3D velocity field v=(vx, vy, vz) can be reduced to 2D given by the averaged velocity vector v=(vx, vy). The mean velocities vx and vy in x and y direction, respectively, are the functions of only x and y coordinates. Using the above-mentioned assumptions, a momentum equation for the single planar channel is obtained, see Equation below:

$$0 = \eta \nabla^2 \overline{v} - \frac{12\eta\overline{v}}{h^2} - \nabla\overline{p} \tag{3.27}$$

Here p denotes the mean pressure averaged along z and the function of x and y. The middle term in this equation results from the averaging procedure. It represents a viscous contribution of the top and bottom channel wall. Eq. (2.2), expressed using individual velocity vector components, gives by substracting Equations shown below

$$0 = \eta(\frac{\partial^2 \overline{v^x}}{\partial \overline{x}^2} + \frac{\partial^2 \overline{v^x}}{\partial \overline{y}^2}) - \frac{12\eta\overline{v^x}}{h^2} - \frac{\partial \overline{p}}{\partial \overline{x}} 0 = \eta(\frac{\partial^2 \overline{v^y}}{\partial \overline{x}^2} + \frac{\partial^2 \overline{v^y}}{\partial \overline{y}^2}) - \frac{12\eta\overline{v^y}}{h^2} - \frac{\partial \overline{p}}{\partial \overline{y}} \tag{3.28}$$

Above equations describe the 2D flow in-between two parallel plates.

Chapter 4

Experimental Setup And Program

In the present investigation, the flow behavior has been studied for existing parallel-cum-series type flow pattern ED unit. The set up was developed to study the flow behavior in the three stages connected in series while in each stage numbers of compartments are arranged in parallel. Flow behavior inside the single compartment with existing and proposed design has also been studied. An ED stack was packed with 75 cell pairs of heterogeneous cation and anion-exchange membranes. This chapter discusses the detail design description about the ED unit and its flow pattern, experimental set ups, and experimental procedure.

4.1 Construction and Working Principle of Existing ED Unite

Parallel-cum-series flow patterns with three stages; stage I, II and III consisting of 30, 25 and 18 cell pairs,respectively, in the stack. A schematic diagram of the experimental stack along with its stages and flow patterns is shown in Fig. 4.1. All other components like electrodes (anode and cathode), gaskets, electrode housing, spacer gasket, etc. were discussed in the previous chapter. One cell pair of ED stack as shown in Fig.4.2consists of two compartments, one treated and other rejected. It includes two cation exchange membranes (thickness 0.13mm) and one anion exchange membrane(thickness- 0.14mm). The membranes are hold in the membrane holding gasket (thickness- 0.4mm) and in between two membranes spacer gasket (thickness- 0.8mm) is provided for effective flow of liquid solution (in present study water).The spacer gasket with woven type net was provided, which creates turbulence inside the compartment.

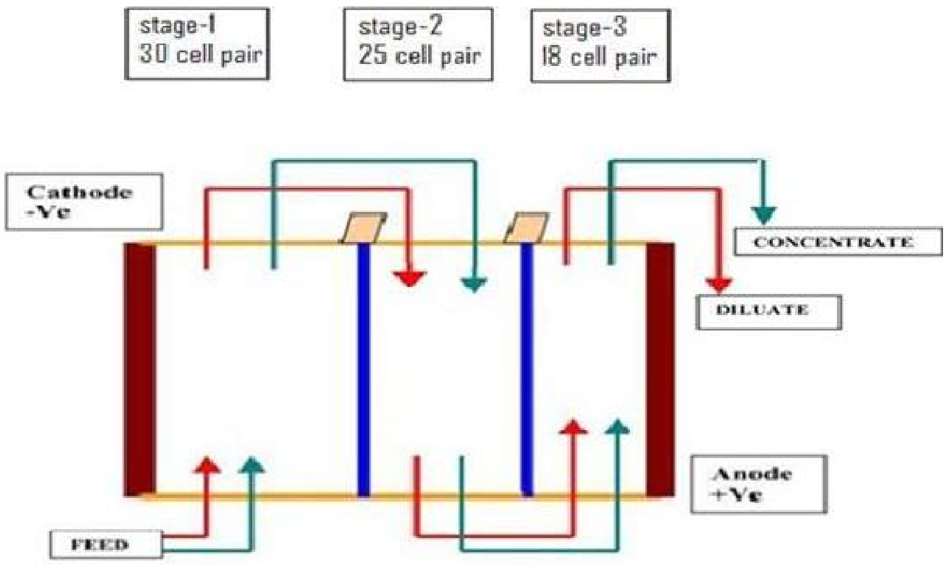

Figure 4.1: Arrangement of stages and flow pattern in existing ED unit

The detailed dimensions and other operating parameters of the ED unit are given in Table I. The ED unit consist 75 compartments for treated and rejected water across three stages.The gaskets were arranged in such a way that the treated inlet water can pass only in the alternate treated compartment through treated inlet header in each stage and concentrated water in the alternate concentrated compartments through concentrate inlet header in each stage. Water from the treated inlet header flows in the treated compartments and from the rejected inlet header flows in rejected compartment in each stage. Water flows from the treated compartments and

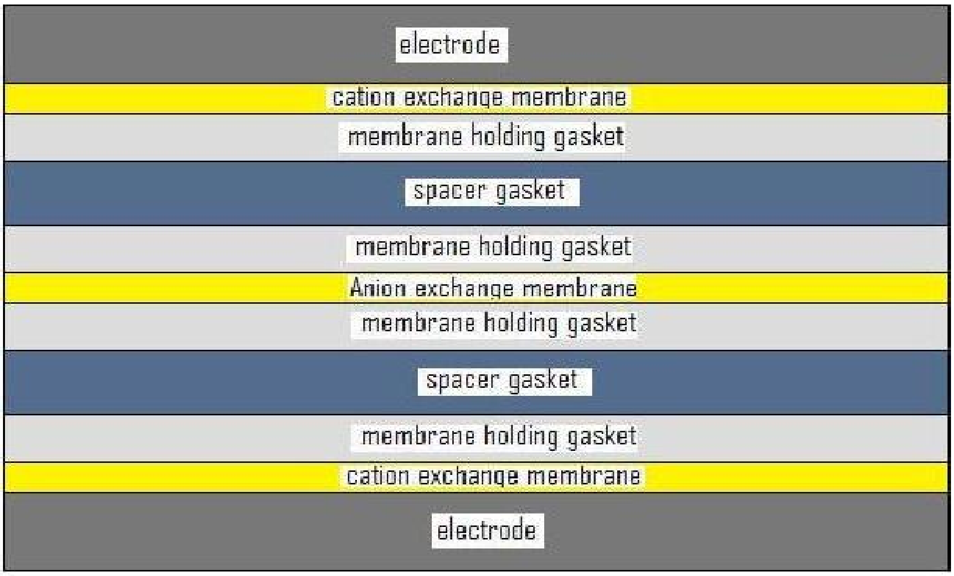

Figure 4.2: Construction of a cell pair

rejected compartments is collected separately through the respective outlet header. The treated compartment in the ED stack is bound by an anion exchange membrane (AEM) facing the positively charged anode and a cation exchange membrane (CEM) facing the negatively charged cathode as shown in Fig. 4.2. The concentrated compartments are bound by AEM facing the cathode and CEM facing the anode as shown in Fig. 4.2. The size and arrangement of holes of anion exchange membranes (AEM), cation exchange membranes (CEM) and membrane holding gaskets are kept similar to the PVC gasket.The electrode housings with electrode are shown in fig 4.3 and 4.4, PVC spacer gasket, membrane holding gaskets and membranes are packed in the pressing assembly with nut-bolts. When electric field is applied, ions in water are attracted to their respective counter electrodes. Thus the diluting compartments are depleted of ions and concentrated compartments are enriched with ions. The salient features of ED stack are given in Table I developed at CSMCRI Bhavnagar. The detailed dimensions of one cell pair are given as;

- Height of one cell pair is = 3.62 mm

- Height of I stage= Number of cell pair in I stage x thickness of one cell pair=

Table I: Details of the ED unit

Parameter	**Characteristics**
Number of cell pairs	75
One cell pair	Two cation exchange membranes, one anion exchange membrane, two spacer gaskets , four membrane holding gaskets
Cell pair thickness	3.62 mm
Type of membranes	Inter polymer type cation and anion exchange membrane
Length of membrane	520 mm
Width of membrane	220 mm
Active area length	380 mm
Active area width	150 mm
Cation exchange membrane thickness	0.14 mm
Anion exchange membrane thickness	0.12 mm
Membrane holding gasket thickness	0.4 mm
Spacer gasket thickness	0.8 mm
Total area of each membrane	114,400 mm2
Effective area of each membrane	57,000 mm2
Spacer Gaskets	Built in flow arrangements and spacers from rigid PVC plate
Electrodes	Expanded platinum coated titanium with precious metal oxide
Electrode housings	Rigid PVC with built inlet and outlet flow distributors
Pressing assembly	Threaded rods with nuts for making stack leak proof
Flow arrangement	Parallel-cum-series
No. of stages	3
Cell pair in each stage respectively	30, 25, 18
Height of each stage respectively	108.6 mm, 90.5 mm, 65.16 mm
Total height of ED stack	271.5 mm

30 x 3.62 = 108.6 mm

- Height of II stage= Number of cell pair in II stage x thickness of one cell pair= 25 x 3.62 = 90.5 mm

- Height of III stage= Number of cell pair in III stage x thickness of one cell pair = 18 x 3.62 = 65.16 mm

- Total height of ED stack= 75 cell pair x thickness of one cell pair= 271.5 mm

The liquid was stored in a tank and was pumped to the treated and rejected compartments.The required electric potential was applied between two electrodes of the ED unit. After attaining steady current in ED stack, the product (treated) water, concentrate (rejected) water and electrode wash were collected for TDS analysis. A small quantity of brackish water at optimum flow rate was passed through electrode compartments to remove the products of electrolysis, process called as electrode wash. Since in the anode compartment acidity was produced due to electrolysis, hence electrode wash was passed first through anode compartment then through cathode compartment to reduce scaling in that compartment.

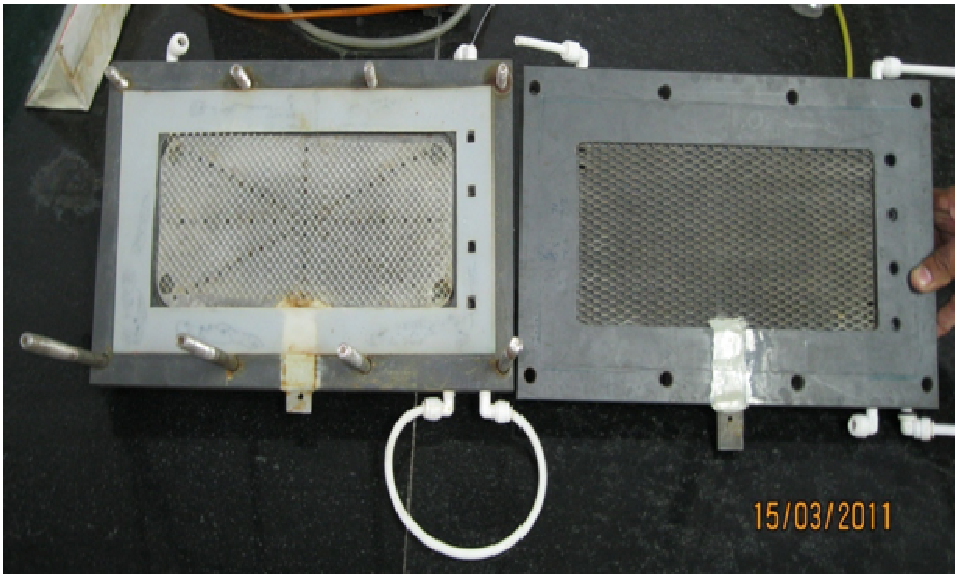

Figure 4.3: photographic view Anode and Cathode plate of ED stack

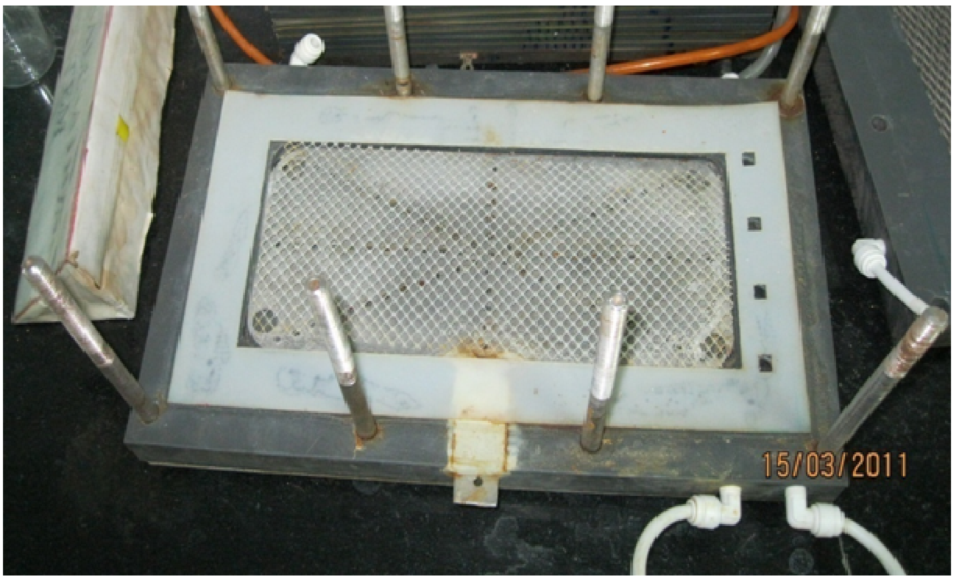

Figure 4.4: photographic view of ED stack housing frame

4.2 Experimental Procedure

Experiments have been conducted using existing ED unit, tap water of same quality was passed through the treated and rejected compartments and electrical potential was applied to the electrode plates. The pressure drop in the ED unit was measured in between inlet and outlet of treated compartments using U-tube manometer. Also the mass flow rate from the treated compartment was measured at outlet.

4.2.1 Investigation for treated compartment

The flow of water in the ED unit is through the treated and rejected compartments. However, in the present investigation, only the treated compartment has been consider for further analysis. As the flow pattern for treated and rejected compartments is same because all the dimensional parameters for header, channel, compartment thickness, etc. are same. Only the changes are in the positioning of inlet and outlet of channels for the treated and rejected compartments.

4.2.2 Pressure Measured using manometer

The manometer consists of U-shape glass tube as shown in Fig.4.5 was fabricated in glassblowing section of CSMCRI Bhavnagar.The U tube manometer was connected to the inlet and outlet of the treated compartments of the ED unit as shown in Fig.4.6 and fig.4.7(Experimental set-up), to measure the pressure difference.

Figure 4.5: Glass U-Tube Manometer

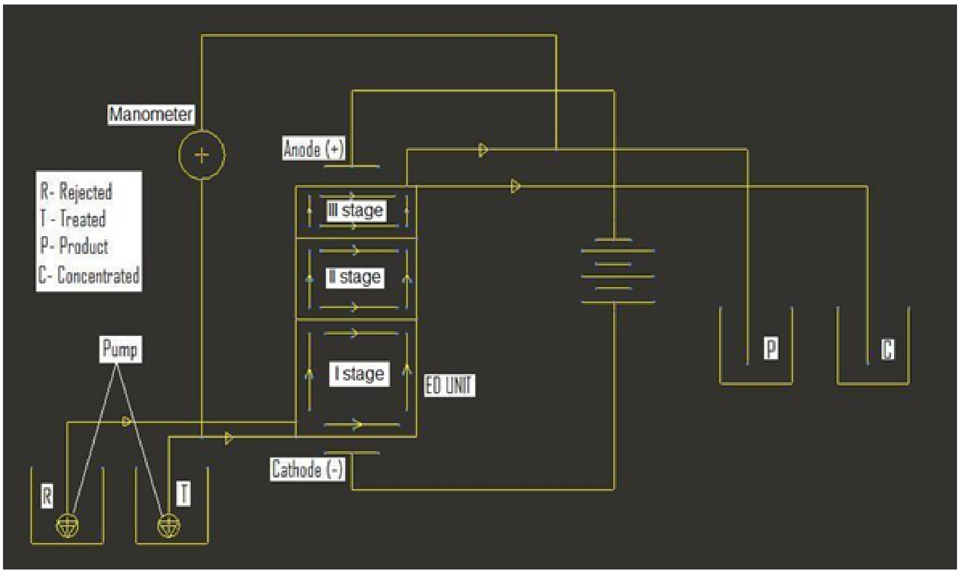

Figure 4.6: schematic diagram of Experimental set-up

Figure 4.7: Experimental set-up

4.3 Experimental Setups for Flow Visualization

Since, the flow inside the ED unit cannot be visualized due to its construction using non transparent membranes and electrode housing. Accordingly, two separate experimental set ups were designed and fabricated to observe the flow behavior in the stages of the ED unit and in the single compartment.

4.3.1 Experimental Set up for Flow Visualization in the Stages of ED unit

The experimental set up as shown in Fig. 4.8 was fabricated for visual observations. Due to constraint of the time and material involved in fabricating the similar model of ED unit a two dimensional model at reduced scale was developed. The set up consists of three stages to study the flow pattern through the compartments.

Figure 4.8: The experimental set up of different stages in ED stack for visual observations

Perspex sheet was used to create the channels with parallel and series arrangement with common inlet and outlet for each stage. Another plain perspex sheet was fixed to the channel fabricated sheet to make it close and leak proof. One inlet and one outlet were provided to flow water. Also at inlet 'T' joint was provided to pass the color solution to study the flow characteristics of the stages.

4.3.2 Experimental Set up for Flow Visualization in the Compartment

Another two separate experimental set ups were fabricated to observe the flow pattern inside the compartment for existing design and new proposed design as shown in Fig. 4.10 and 4.12 and detail drawing view of spacer gasket is shown in Fig 4.9 and4.11.Instead of two membranes, two transparent polypropylene sheets were fixed with nut and bolts. The gap between the two polypropylene sheets was maintained by inserting the membrane holding and spacer gaskets. Two inlets and two outlets as provided in the compartment of actual ED unit were provided to flow the water inside the compartment.Also a provision of 'T' joint was made to pass colour solution to identify the flow patterns.

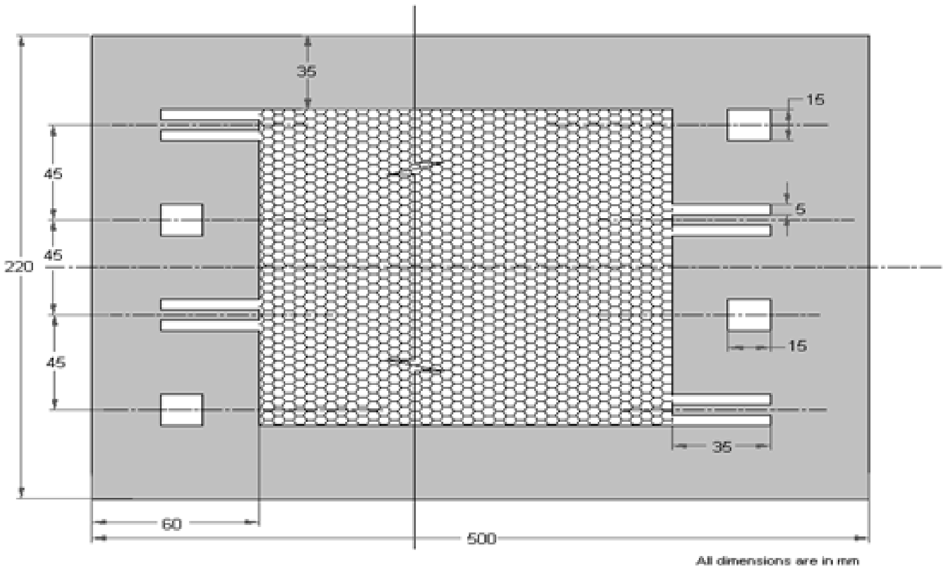

Figure 4.9: Existing design of spacer gasket

Figure 4.10: Experimental set-up of single existing compartment for flow visualization

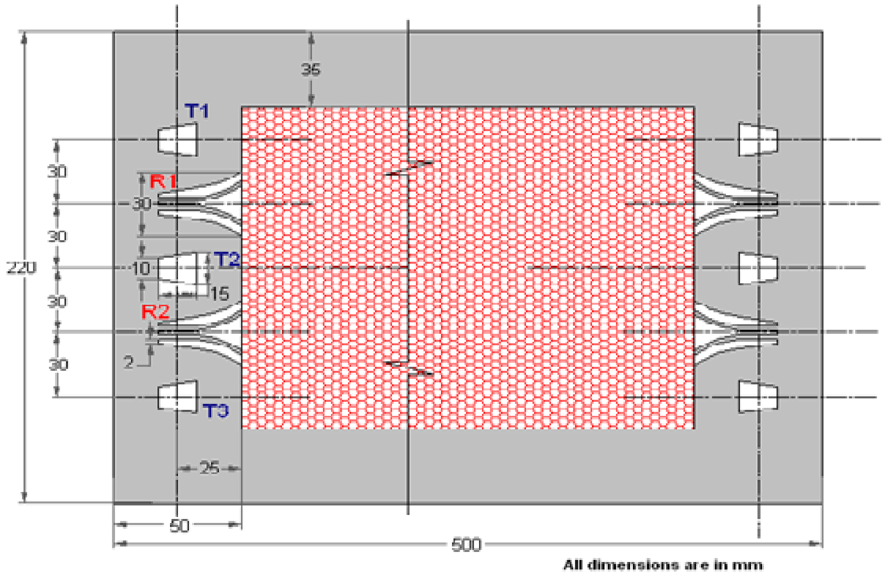

Figure 4.11: Proposed design of spacer gasket

Figure 4.12: Experimental set-up of single proposed compartment for flow visualization

Chapter 5

CFD Based Flow Analysis Of ED Stack

Basics of CFD and steps for the numerical simulation of the problem are discussed in chapter 3. This chapter presents the detailed methodology adopted to carry out the numerical simulation of ED stack and its compartments in different stages using commercial Navier-Stokes codes called 'FLUENT'. In this chapter, the steps for the creation of 2-D computational geometry of ED stack and its compartments in different stages in GAMBIT are described. Details of grid generation and zone specification are given. The simulation technique adopted in FLUENT and details of laminar models used are described.

5.1 Introduction of ED stack

The water flow inside the treated and rejected compartments and electrode wash in the ED stack is a complex phenomenon due to parallel and series flow arrangements of compartments. It becomes more tedious and unpredictable with reference to the transportation of ions from concentrated to treated one.

In ED process, the flow of water over the surface of the membranes, plays an important role in overall stack resistance, desalting performance, energy consumption, current

efficiency etc. that ultimately determine the capital cost and product water cost.
The important parameters namely, flow distribution in the compartments, effect of spacer gasket geometry, water distribution through channels, pressure drop, velocity, etc. were analyzed using the CFD. The demand for efficient and cost effective design of ED stack in industries is rapidly increasing. In industries different types of ED stacks are designed and developed to improve efficiency and cost effectiveness. A number of industries are interested in ED stack for different industrial processes namely, water purification, effluent treatment, desalination of chemicals, recovery of valuable chemicals, etc. As per the industries requirements the design of the ED stack varies significantly for its effective use.
In the present investigation, the ED stack having capacity of 252 lit/hr developed at CSMCRI,Bhavnagar is considered for CFD analysis. The detailed specifications and drawings of the ED stack are given in detail in previous chapter. The ED stack consists of three stages in series with total 75 cell pairs. These cell pairs are arranged in parallel, 30 cell pairs in first stage, 25 cell pairs in second and 18 cell pairs in third stage.

5.2 Computational Modeling

The computational modeling, meshing of the geometry and specifying zones are initial steps in CFD analysis. These three steps are performed in GAMBIT, which is a pre-processor of FLUENT. The complete methodology applied for the computational modeling, meshing and ED stack and compartments are described in following paragraphs.

5.2.1 Geometry creation using Gambit

5.2.1.1 ED stack Geometry Creation

The geometries of the different components (i.e. inlet section, outlet section, three stages, and channel in each stage) are created in the pre-processor called GAMBIT.

The hierarchy of geometric objects in GAMBIT is Vertices→Edges→Faces. This approach is called Bottom-up approach. Initially, the geometry of the component i.e. ED stack is created and its details are as follow:

5.2.1.1.1 ED stack (3 stage parallel-cum-series pattern) module

The ED compartment is divided into three different sections and three sections are of different sizes and the steps are as follow:

a. Create three different sections.

  - One inlet header
  - The middle section of ED stack channels(in series)/compartments in three parallel stages (Active area)
  - One outlet header (the dimensions of all nozzles at inlet and outlet are same)

b. Create the number of faces between successive sections All the vertexes of inlet section, channel section (active area) and outlet section are joined together. The complete ED stack design after joining all the edges converted into faces in GAMBIT is shown in FIG.5.1.

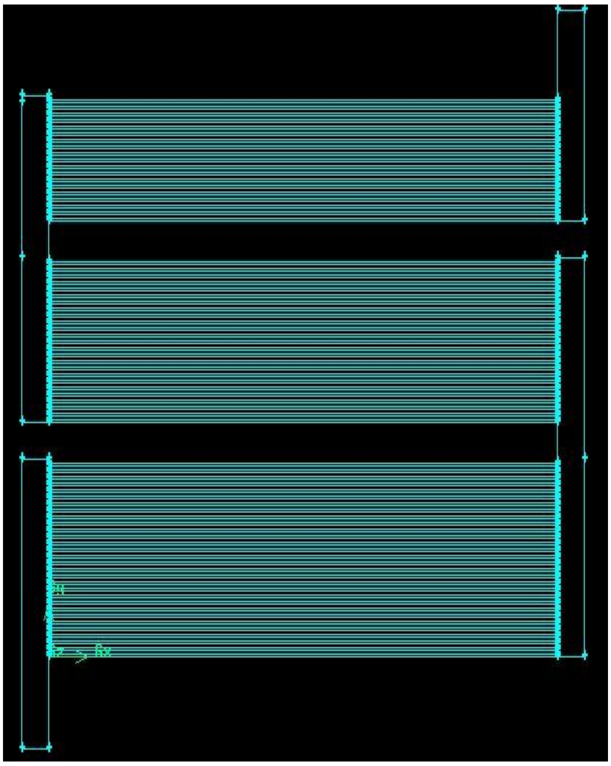

Figure 5.1: ED stack (three stages parallel-cum-series ED stack)

5.2.1.1.2 ED stack (one stage, straight inlet header)

As one stage (parallel channels) ED stack is created as discussed in last point 5.2.1.1.1 only considering one stage in middle section. Purpose of modeling one stage is to make study easier of parallel channel flow in CFD and to reduce the time taken in the analysis by Fluent. Fig.5.2 shows the one stage ED stack with straight inlet header.

5.2.1.1.3 ED stack (One stage, Trapezoidal inlet header)

The parallel compartments arrangement of first stage of ED stack is created and discussed in point 5.2.1.1.2. Changes have been made only in modeling of inlet header. Straight inlet header has been replaced by trapezoidal shape for proposed design while other all parameters were kept same. Total area of the inlet header of trapezoidal design has been same as inlet header of straight design. Fig.5.3 shows the first stage of ED stack with trapezoidal inlet header.

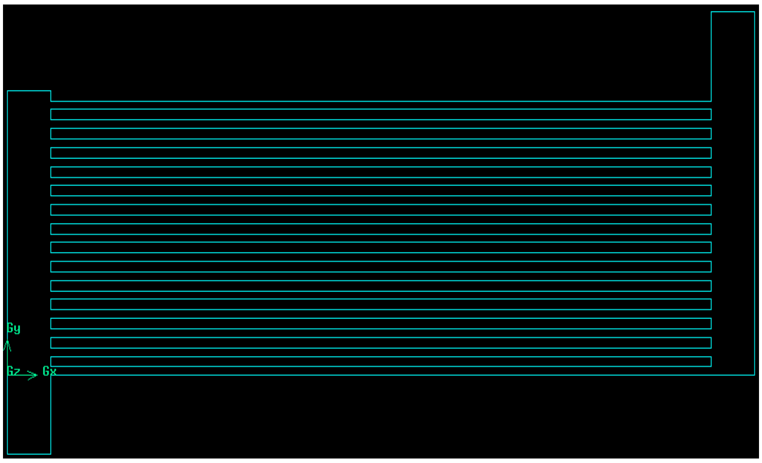

Figure 5.2: One stage ED stack with straight header

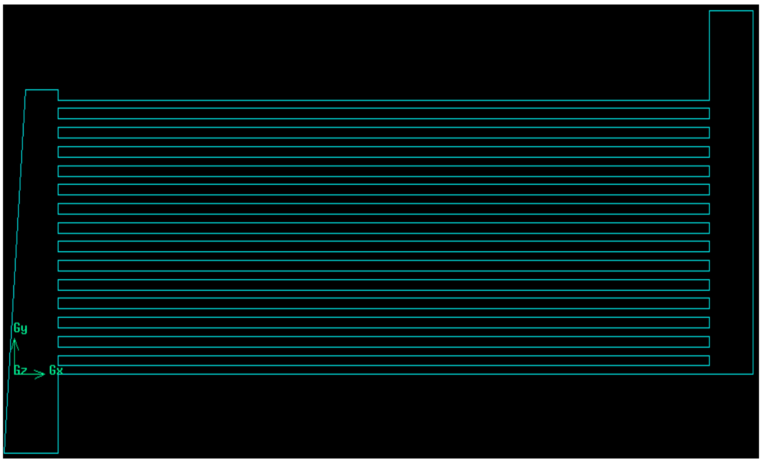

Figure 5.3: one stage ED stack with trapezoidal header

5.2.1.2 Compartment Geometry Creation

The geometries of the different components (i.e. inlet section, outlet section and active area of ED comportment) are created in the pre-processor called GAMBIT. The hierarchy of geometric objects in GAMBIT is Vertices ' Edges' Faces. This approach is called Bottom-up approach. Initially, the geometry of the component i.e. ED compartment is created and its details are given as follow:

ED compartment module plate

The ED compartment is divided into three different sections and three sections are of different sizes and the steps are as follow:

a. Create three different sections.

- Two inlet nozzles
- The middle section of compartment/plate having channel (Active area)
- Two outlet nozzles (the dimensions of all nozzles at inlet and outlet are same)

b. Create the number of faces between successive sections All the vertexes of inlet section, channel section (active area) and outlet section are joined together. The complete ED compartments design after joining all the edges converted into faces in GAMBIT are shown in Figs. **??**and **??** for the existing and for the proposed design of the compartments, respectively.

Figure 5.4: Existing design of compartment

Figure 5.5: Proposed design of compartment

5.2.2 Grid Generation and Zone specification

5.2.2.1 Grid generation

One of the most important and time-consuming challenge in the CFD simulation process is the generation of the computational grid or mesh. As the geometry is complex the unstructured grid is used with square and tetrahedral elements. The size of the element during meshing defines the ability to solve the problem and its accuracy. The parameter size function controls the size of mesh intervals for edges and meshing elements at faces. Size functions are similar to boundary layers in that they control the mesh characteristics in the proximity of the entities to which they are attached. They differ from boundary layers with respect to the manner in which they are defined and the manner in which they control the mesh. Whereas boundary layers prescribe specific mesh patterns and the sizes of mesh elements within those patterns.

The steps for grid generation:

a. Mesh the whole face of ED stack and compartment with different appropriate scheme.

b. Examine the mesh quality for equi-size and equi-angle skewness elements.

The geometry generated using this different goods in GAMBIT, are shown in Figs.5.6,5.7, 5.8, 5.9,and 5.10 for existing and proposed designs of ED stack (III stage,I stage) and compartments, respectively.

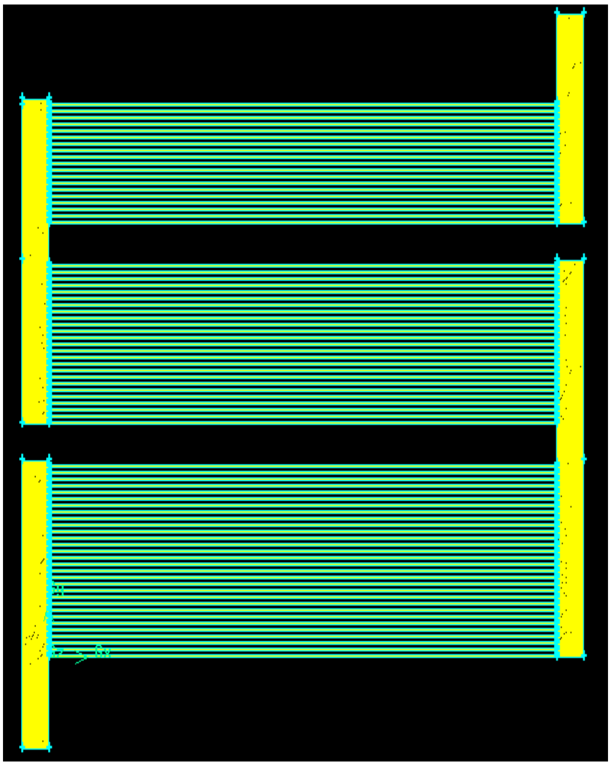

Figure 5.6: Quad/Tri Pave Type grid in III stage ED stack design

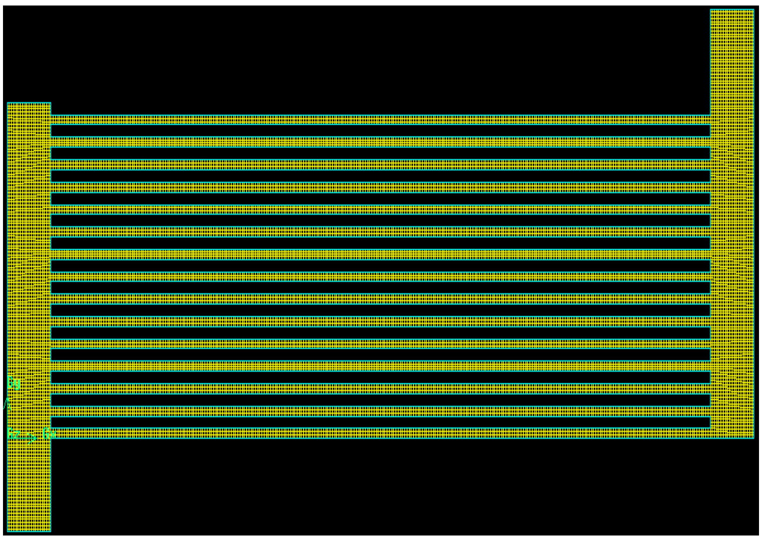

Figure 5.7: Quad Pave Type grid in existing ED stack (I stage) design

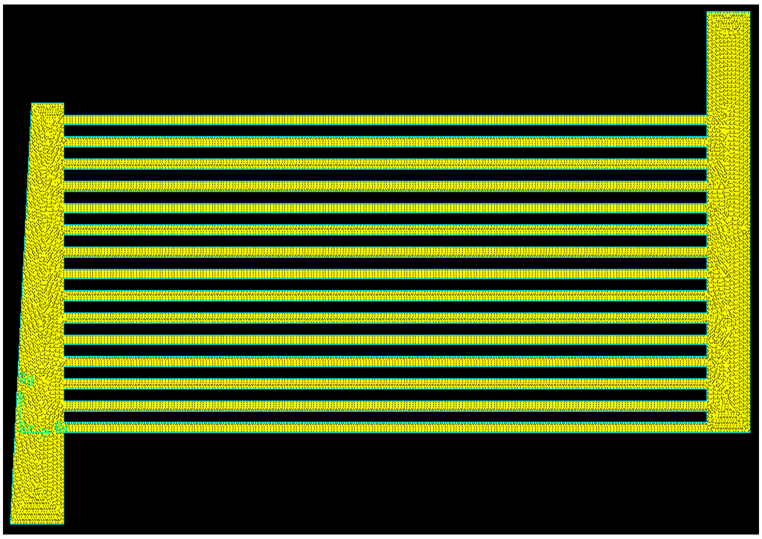

Figure 5.8: Quad/Tri Pave Type grid in proposed ED stack (I stage) design

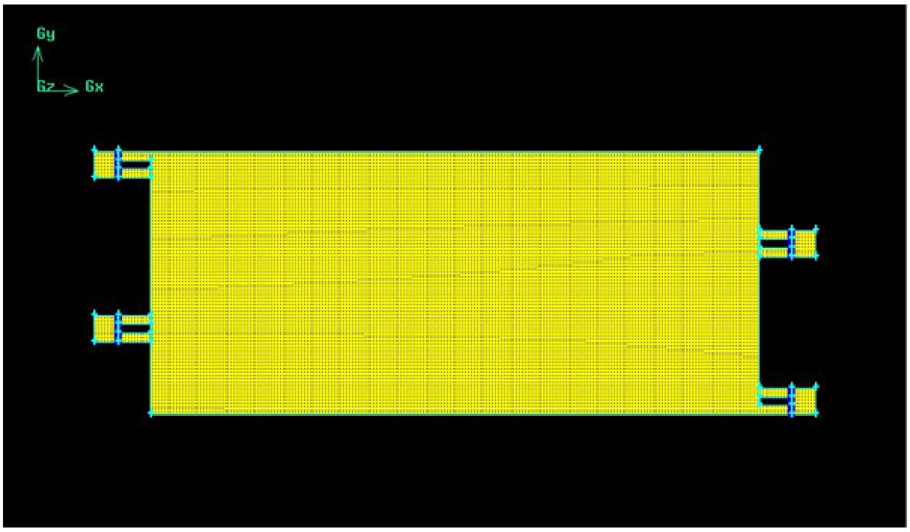

Figure 5.9: Quad Pave type grid in Existing design of compartment

Figure 5.10: Quad/Tri Pave Type grid in Proposed design of compartment

5.2.2.2 Zone specification

Zone specifications are used to define the physical and operational characteristics of the model at its boundaries and within specific regions of its domain. The zone specifications are classified as Boundary types and Continuum types. Before exporting the mesh geometry to FLUENT, it is required to specify the zone types in GAMBIT and described in detail as;

a. Boundary type

   Boundary-type specifications, such as VELOCITY INLET, PRESSURE INLET AND OUTLET and WALL define the characteristics of the model at its internal and external boundaries respectively. The boundary types used in the present investigation are specified as;

   - At inlet: Pressure Inlet
   - Walls : no slip
   - Other than the water flow edges considered as default interior
   - At outlet: Pressure Outlet

b. Continuum type

   Continuum-type specifications, such as FLUID define the characteristics of the model within specified regions of its domain. The continuum types used in the present investigation are specified as;

   - a. Inlet, Outlet and Active area of Stack and compartment : Fluid

   After completing the modeling, meshing and specifying zones with boundary conditions in GAMBIT, the entire mesh is exported to 'FLUENT 5/6 Solver' for simulation.

5.2.3 Simulation in FLUENT

The predictions of the complex flow inside the ED stack and compartment can be achieved significantly using CFD. These predictions are supportive while designing the ED stack and compartment. This article describes the 2-dimensional (2d) simulation of flow in the stack and compartments. A commercial available 2d Navier-Stokes code called 'FLUENT' with laminar model is used to simulate the flow conditions. Finite Volume method (FVM) is used for the discretization of governing equations. To avoid the more complexity, better understanding of the flow profile and to have better predictions, certain assumptions made during the simulation of flow conditions are given below as;

a. Flow is steady state.

b. Fluid is incompressible.

c. Fluid properties are constant.

d. No vapor is present in the water, i.e. single phase flow.

e. There is no leakage in the plate.

f. The surface of all the components are hydraulically smooth.

g. No mass (fluid and/or ions) transfer from the compartment through the active area (i.e. through membrane).

h. Compartment without spacer gasket.

5.3 Solution Technique

Generally, single precision version or double precision version computational facilities available with FLUENT's are used for simulation. In the present investigation, the double precision version computational facility is used due to more accuracy and capacity to round-off errors. The different steps involved in computation are given below as;

a. The grid is read and checked in FLUENT.

b. Whole Grid is scaled in any one unit (meter, cm, mm, in, ft)

c. Smoothing swapping of grid done

d. The segregated implicit solver with absolute velocity formulation is used for the computation. The cell-based gradient scheme is used which is more accurate than the cell-based scheme for structured meshes, most notably for quadrilateral meshes.

e. Water with following properties is used as a working fluid.(Density = 998.2 kg/m3,Viscosity = 0.001003 kg/m-s)

f. Initial and boundary condition applying at outlet of inlet nozzle and inlet of outlet nozzle.

   - Initial condition : 101325 N/m2
   - Boundary conditions: working fluid is fluid and inlet and outlet values are given.

g. Following convergence criteria is used for different equations.

   - Continuity equation 0.0001
   - Momentum equations 0.0001

h. A SIMPLE scheme is used for the pressure velocity coupling.

i. For pressure correction, STANDARD scheme is used which is suitable for static pressure problems.

j. For momentum and turbulence, first order upwind scheme is used.

k. Initially, following under relaxation factors are used.

- Pressure 0.5
- Momentum 0.2

Now the boundary conditions are required to define and apply to the problem through FLUENT. These boundary conditions are defined either by using experimental data or from calculations.

Chapter 6

Results and Discussion

The desalination rate of any quality of water or chemical of the ED unit depends on the parameter namely, properties of membrane, applied voltage, current density, thickness of the compartment, active area of the membrane, effective area of the membrane, mass flow rate of fed water, velocity of the water in inlet and outlet headers and compartments, compartments arrangement and number of stages, etc. The ED stack fabricated using the ion exchange membrane developed at CSMCRI, Bhavnagar has been used in the present investigation.

Normal tap water is fed in two separate streams to treated and rejected inlets of ED unit. The flow inside the ED unit is complex and involves lot of fluid mechanics, the effect of parameters namely; pressure drop, water flow rate (distribution) and its velocity can be investigated using numerical methods [1]. These parameters are mainly depend on the inlet and outlet header, number of stages and number of compartments in each stages. These conditions significantly affect the effective membrane area from the active area of compartment for ion transportation. The mass flow rate and velocity of water cannot predict the exact distribution of water inside the each and every compartment (i.e in parallel channels). In the parallel channel flow arrangements the fluid finds the least resistance path and may create the back pressure which affects the flow in other compartments and consequently reduces the water flow. Thus water flow inside the compartment may follow the least resistance path without covering the maximum area inside the compartment and similarly, the other compartments where flow is minimum, both reduces the efficiency of the ED stack. Due to this, ions will not have sufficient time to get transport from treated compartment to rejected one. Thus the improvement in the design of inlet and outlet section of each compartment is responsible for flow distribution vis--vis maximize the effective area of membrane which significantly improves transportation of ions.

6.1 Experimental Results

The schematic diagram of the experimental set up consists of ED unit equipped with manometer as shown in Fig.4.7 was used to determine the pressure drop across the inlet and outlet of the ED stack. A conventional Bernoulli equation was used to calculate the velocity for three stages and further the velocity inside the compartment and at inlet and outlet was calculated (assuming equal mass flow rate in each compartment). It is observed that the total pressure drop in the ED stack is 10548.979 N/m2 (1.53 psi). The water mass flow rates for the treated inlet and outlet is measured using measuring flask and stop watch. It is observed around 252 liter/hr from the ED stack.

6.2 Theoretical Calculations

Based on the experimental results and other known properties of liquid the following calculation are done to calculate the pressure and velocity at different locations:

6.2.1 ED stack calculations

The area of inlet and outlet header and its openings to each stage and area of compartments was calculated and based on calculated pressure across each stage velocity at respective points is calculated and given in TableII.

6.2.1.1 Pressure calculations:

a. **Pressure at inlet:**

h_w=height of water replace the mercury= 0.44 m

h_{hg}=height of mercury displaced= 0.11 m

P_{atm}=atmospheric pressure= 101325.25 N/m^2

P_{in}=Pressure at the treated inlet of ED unit

ρ_w,ρ_{hg}=density of water and mercury, respectively

$P_{in} + (\rho \times g \times h)_w = (\rho \times g \times h)_{hg} + P_{atm}$

$P_{in} + (1000 \times 9.81 \times 0.44)_w = (13600 \times 9.81 \times 0.11)_{hg} + 101325$

$P_{in} = 111659.36 N/m^2$= 16.19 psi

b. **Pressure at outlet of ED stack:**

P_{out}=101077.145 N/m^2= 14.66 psi

c. **Pressure drop of ED stack:**

ΔP_s= P_{in}- P_{out}= 10548.979 N/m^2= 1.53 psi

ΔP calculated mathematically depending on number of cellpair across each stage: I stage=Δ P_1=4219.59 N/m^2

II stage=Δ P_2=3516.33 N/m^2

III stage=Δ $P3$=2530.38 N/m^2

d. **Pressure at each stage Outlet:**

I stage=P_1=107439.77 N/m^2

II stage=P_2=103923.44N/m^2

III stage=P_3=101393.06 N/m^2

6.2.1.2 Area calculations:

a. 'A' TYPE OPENING:(Membrane holding gasket(MHG) and Membrane)

Area of 'A' type opening A_A= 15 $\times$ 15 mm^2 = 225 mm^2

Perimeter of 'A' type opening (P_A)= 60 mm

Hydraulic Diameter for 'A' type D_{hA}= $(4 \times A_A)/P_A$ = 15 mm

Hydraulic Area for 'A' type A_{hA}= $\frac{\Pi}{4} \times (D_{hA})^2 = 176.6\ mm^2$

b. 'B' TYPE OPENING:(Spacer gasket (SG))

Area of 'B' type opening (A_B)= $5 \times 15\ mm^2 = 75\ mm^2$

Perimeter of 'B' type opening (P_B)= 40 mm

Hydraulic Diameter for 'B' type (D_hB)=$(4 \times A_B)/P_B$ = 7.5 mm

Hydraulic Area for 'B' type A_{hB}=$\frac{\Pi}{4} \times (D_{hB})^2 = 44.15\ mm^2$

6.2.1.3 Velocity calculations

Mass flow rate is experimentally measured by using flask and stopwatch at the inlet and outlet of the ED unit. It was measured 252 litre/hr.

Mass flow rate at inlet of ED stack = 252 litre/hr = 0.07 litre/sec

Velocity at inlet of unit (V_s)= $[m_s\ /\ (\rho \times D_e)]$= 0.592 m/s

6.2.2 First stage calculations

6.2.2.1 Pressure calculation

ED stack pressure drop(ΔP_s)= 10548.979 N/m2

I stage pressure drop (ΔP_1)= ΔP_s / Number of cell pair in I stage

ΔP_1= 10548.979/ 30= 4219.59 N/m^2

P_{out}= P_{in} - ΔP_1= 111659.36 - 4219.59= 107439.77 N/m^2

6.2.2.2 Area calculation

'A' Type openings: (Gasket + Membrane holding gasket)

Length of gasket:

= Number of cell pair in 1^{st} stage × no. of gasket in one cell pair × thickness of one gasket

$= 40 \times 4 \times 0.4$

= 48 mm

Length of membranes:

= No. of cell pair in 1^{st} stage × no. of gasket in one cell pair × thickness of one gasket

$= 30 \times 3 \times 0.14$

= 12.6 mm

Length of 'A' type opening (L_A):= length of gasket + length membranes

$L_A = 48 + 12.6$

= 60.6 mm

Volume (V_A)= $A_{hA} \times L_A$

$= 176.6 \times 60.6 = 10701.96\ mm^3$

'B' type openings: (Spacer gasket)

Length of 'B' type opening L_B:

= no. of cell pair × no. of spacer gasket in one cell pair × thickness of one spacer gasket

$L_B = 30 \times 2 \times 0.8 = 48$ mm

Volume (V_B):= $A_{hB} \times L_B = 44.15 \times 48$

$V_B = 2119.2\ mm^3$

Now, the equivalent diameter from "A" and "B" type opening is calculated as;

Equivalent volume V_e= V_A + V_B= 10701.96 + 2119.2

V_e= 12821.16 mm^3

Total length L_T= L_A + L_B

L_T= 108.6 mm

Equivalent Area A_e= V_e/L_T

A_e= 118.05 mm^2

Equivalent diameter D_e= $[(4 \times Ae)/\Pi]^{1/2}$

D_e= 12.26 mm

6.2.2.3 Velocity calculation

Mass flow rate (m_{1s})= 252 kg/hr= 0.07 kg/sec

Velocity (V_{1s})= $[m_{1s}/(\rho \times D_e)]$= 0.592 m/s

6.2.3 Pressure, Velocity and Area Calculations for Compartments:

The velocity and pressure at different locations for the compartment of first stage are calculated by assuming equal mass of water flowing through all the compartments.

Mass flow rate through each compartment of I stage (m_{1c}):

(Assume equal mass flow in all 30 compartments of 1st stage)

m_{1c}= m_s/No. of compartment in I stage = 252/30 = 8.4 kg/hr

m_{1c}= 0.0023 kg/sec

6.2.3.1 Area calculations:

Area of inlet opening to compartment

Total area (A_c)=no. of openings $\times$ thickness $\times$ width

A_c= 4 $\times$ 0.8 $\times$ 5 = 16 mm^2

Total perimeter P_c= no. openings $\times$ perimeter of one opening

P_c= 4 $\times$ [2 $\times$ (5 + 0.8)]= 11.6 mm

Hydraulic diameter d_{hc}= [(4 $\times$ ($\frac{A_c}{P_c}$)]= 1.37 mm

Hydraulic area A_{hc}= 4 $\times$ 1.372= 1.47 mm^2

6.2.3.2 Velocity Calculations for the Compartment (without head loss):

a. Inlet velocity of the compartment (V_{ci}):

   V_{ci}= [m_{1c} /(ρ $\times$ A_{hc})]

   V_{ci}= 1.58 m/s

b. Velocity at any point in the flow area of compartment: (V_{cp})

   (Assumption equal flow velocity throughout the compartment)

   Area (A_{cp})= 150 $\times$ 1.6 mm^2

   (A_{cp})= 240 mm^2

   Velocity V_{cp}= m_{1c} /(ρ $\times$ A_{cp})

   V_{cp}= 0.00972 m/s

c. Outlet velocity of the compartment (V_{co}):

   Applying Bernoulli's equation,

   $\frac{p_{in}}{\rho} + \frac{(V_{ci})^2}{2} = \frac{p_{out}}{\rho} + \frac{(V_{co})^2}{2}$

Now, $Z_1 = Z_2$

$\frac{p_{in}}{1000} - \frac{p_{out}}{\rho} = \frac{(V_{co})^2}{2} - \frac{(V_{ci})^2}{2}$

V_{co}= 3.30m/s

6.2.3.3 Velocity Calculations (With head loss):

Total head loss:Major loss + Minor loss

Major loss:Friction loss inside the compartment

Minor loss:Entry loss + Enlargement loss + Contraction loss + Exit loss.

6.2.3.3.1 Major Head Loss Calculation:

Major loss= $\frac{4\times f\times L\times V^2}{2\times g\times d_h}$

Volume of compartment= 0.380 × 0.150 × 0.0016= 9.12 × 10^{-5} m^2

Area of the compartment= 0.057 m^2

Reynold's no.(Re)

Re =$\frac{\rho\times V_{cp}\times d_h}{\mu}$

Re = 62.06

From the empirical correlation of Kays and Crawford:

Re × f = 13.84 + 10.38 exp($\frac{-3.4}{a}$)

a = channel aspect ratio = W_c/b_c= 0.15/ 0.0016= 93.75

So, Re × f= 23.85

f= 0.384

d_h = hydraulic diameter = (4 × A)/ P

=[4 (W_c+b_c)]/ 2(W_c+b_c)= 0.00316

Now,Major friction loss

= $\frac{4\times f\times L\times V^2}{2\times g\times d_h}$= 0.000889

6.2.3.3.2 Minor head loss calculation

Minor loss= entry loss + sudden expansion + contraction + exit loss

V_{ci}= 1.58 m/s,V_{cp}= 0.00972 m/s, V_{co}= 3.30 m/s

A1= area inside the compartment= 240 mm^2

A2= Area of the outlet openings= 1.47 mm^2

Now,**Contraction coefficient Cc**= 0.62+ 0.38 $(A_2/A_1)^2$= 0.62

$\frac{V_{cp}}{V_c} = C_c$

a. Entry loss = $\frac{0.5\times(V_{ci})^2}{2\times g}$= 0.0636

b. Loss due to sudden expansion = $\frac{(V_{ci}-V_{cp})^2}{2\times g}$ = 0.125

c. Loss due to sudde contraction = $\frac{(V_c-V_{cp})^2}{2\times g}$ = 0.208

d. Loss due to exit = $\frac{V^{cp}}{2\times g}$ = 4.81×10^{-6}

Total Minor loss= entry loss +sudden expansion +sudden contraction + exit loss= 0.3936

6.2.3.3.3 Major Head Loss Calculation:

Total head loss (H_f)= major loss + minor loss= 0.000889 + 0.3936

H_f= 0.39449

6.2.3.3.3 Recalculating outlet velocity of the compartment considering head loss:

Applying Bernoulli's equation between inlet and outlet of compartment

$\frac{P_{ci}}{\rho} - \frac{P_{ci}}{\rho} = \frac{(V_{co})^2}{2} - \frac{(V_{ci})^2}{2} + g + H_f$

P_{ci} - P_{co} = Δ P_1= 4219.59N/m^2 and V_{ci}= 1.58 m/s

$\frac{4219.59}{1000} = \frac{(V_{co})^2}{2} - \frac{(1.58)^2}{2} + 9.81 + 0.39449$

$(V_{co})^2 = 3.17$ m/s

$V_{co} = 1.78$ m/s

Thus based on all the calculations made to calculate the head losses for single compartment of first stage are given in TableI. Al the results obtained for the compartments

Table I: Details of head loss for single compartment of first stage

Measured parameter	**Value**
Major losses	0.000889
Entery losses	0.0636
Sudden expansion losses	0.125
Contraction losses	0.208
Exit loss	4.81×10^{-6}
Minor loss	0.3936
Total loss	0.394489
Outlet velocity without considering head loss	3.30 m/s
Outlet velocity considering head loss	1.78 m/s

of first stage are given in Table 6.2. Similarly, the calculations for second (25 number cell pairs) and third (18 number cell pairs) stages are made and the final results are also given in TableII(Area of inlet and outlet openings for the compartments of second and third stages remain same to as of first stage).

Table II: Details of head loss for single compartment of first stage

Parameters measures	I stage	II stage	III stage
Number of cell pair	30	25	18
Pressure drop (ΔP) (N/m^2)	4219.59	3516.33	2530.38
Length of 'A' type opening (L_A) (mm)	60.6	50.6	36.36
Length of 'B' type opening (L_B) (mm)	48	40	28.8
Total length (L_T) (mm)	108.6	90.6	65.16
Volume of 'A' type opening (Vol_A) (mm^3)	10701.96	8935.96	6421.176
Volume of 'B' type opening (Vol_B) (mm^3)	2119.2	1766	1271.52
Total volume ($Vol_e = Vol_A + Vol_B$)(mm^3)	12821.16	10701.96	7692.69
Equivalent Area (A_e) (mm^2)	118.05	118.05	118.05
Equivalent Diameter (D_e) (mm)	12.25	12.26	12.25
mass flow rate at inlet of each stage (m_1,m_1,m_1) (kg/hr)	252	252	252
mass flow rate through each compartment (m_{1c}, m_{2c}, m_{3c}) (kg/hr)	8.4	10.08	14
Hydraulic area (A_{hc}) (mm^2)	1.379	1.379	1.379
Velocity at inlet of compartment (V_{ci}) (m/s)	1.58	1.89	2.63
Velocity at any point inside the compartment (V_cp) (m/s)	0.00972	0.0116	0.0161
Velocity at outlet of the compartment (V_{co}) (m/s)	3.30	3.25	3.46

6.3 Experimental and CFD Results for ED Stack

Due to construction of ED stack using non-transparent components like electrode housing and membranes, it is very difficult to visualise the flow inside the ED stack and also inside the compartments. Thus to overcome this problem an experimental set up was developed and discussed in detail in chapter 4. The flow inside the ED stack has been observed experimentally by injecting the colour die. Apart from that the CFD was used to compute the velocity and pressure in the ED stack. Also the flow behaviour results of the ED stack were computed using CFD and are presented in the following sections.

6.3.1 Flow Pattern in the ED Stack (Experimental results)

The experimental procedure is discussed in Chapter 4, at the time of experimentation photographs of the ED unit were captured after appropriate time interval and are presented in Fig.6.1 (a-f). The Fig.6.1(a) shows the water flow through the channels of various stages. It is very difficult to visualize the live flow in the channels of different stages. To overcome this problem, the flow of water was stopped and dark pink coloured solution was passed (due care was take no air pockets will get developed). Immediately after the supply of coloured solution photograph was captured and presented in Fig.6.1(b). It shows that the colour solution is flowing at high velocity through the inlet header and allows the solution to flow through the upper channels. The similar kind of observation can be seen from Fig.6.1(c) for second stage. Slowly with time the colour solution appears in the upper channels of the first stage. The same observations can also be made from Fig.6.1(d-f). The series of photographs shows the variation in darkness of colour in the channels of three stages. This illustrate that the water flows at high velocity from some channels (dark solution channels) and from few channels water flows at lower velocity (diluted coloured solution channels).

From these observations, it can be concluded that large variations in the flow velocity through the compartments of all stages is occurring. This may be due to the back pressure developed due to high velocity flow through the few compartments. This leads to reduce the efficiency of the both high velocity and low velocity flow compartments. The former one allows the water to flow at high velocity and may not get sufficient time to transfer the ions through membranes, while in later one the flow velocity of water is too low that the ions gets transfer through membrane but cloud not transfer sufficient quantity of ions due to unavailability of ions.

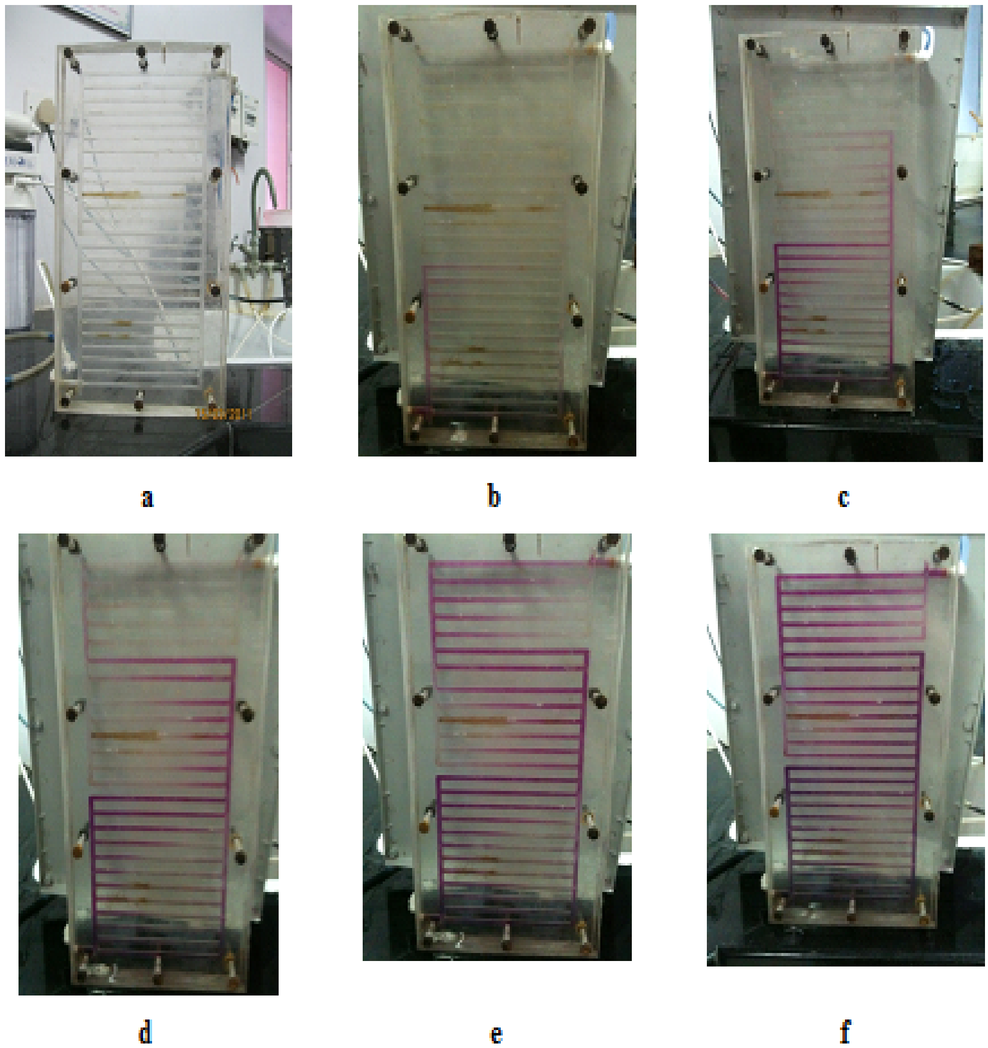

Figure 6.1: Flow visualization in the channels of different stages in ED stack

6.3.2 Flow Analysis of ED Stack using CFD

Experimentally it is difficult to measure the velocity and pressure in the channels of various stages in the ED unit. Thus the complete geometry of the ED stack was analysed using Fluent 6.2. As per the assumptions and boundary condition given in previous chapter the velocity and pressure contours for the ED stack were computed using Navier-Stroke equations for the three stages of ED unit. The velocity and Pressure contours of complete ED stack foe three stages generated using FLUENT are presented in Fig.6.2and Fig.6.3, respectively.

It is observed from the Fig.6.2 that the water flows at higher velocities in the upper channels compare to the lower channels in the three stages. From Fig.6.3, it is observed that the pressure difference between the inlet and outlet header is high at upper side for each stage, while same pressure is observed in the header at lower side. This shows that the large variation in the flow velocity in the compartments of each stage. The similar flow velocity behaviour has been observed experimentally.

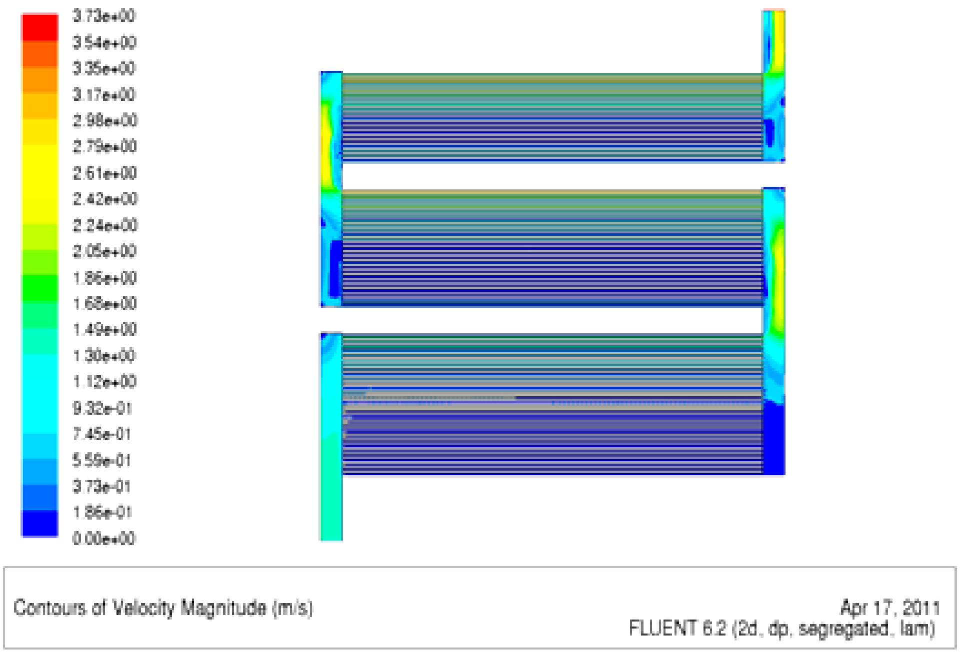

Figure 6.2: Velocity contour for three stages of the ED stack using Fluent

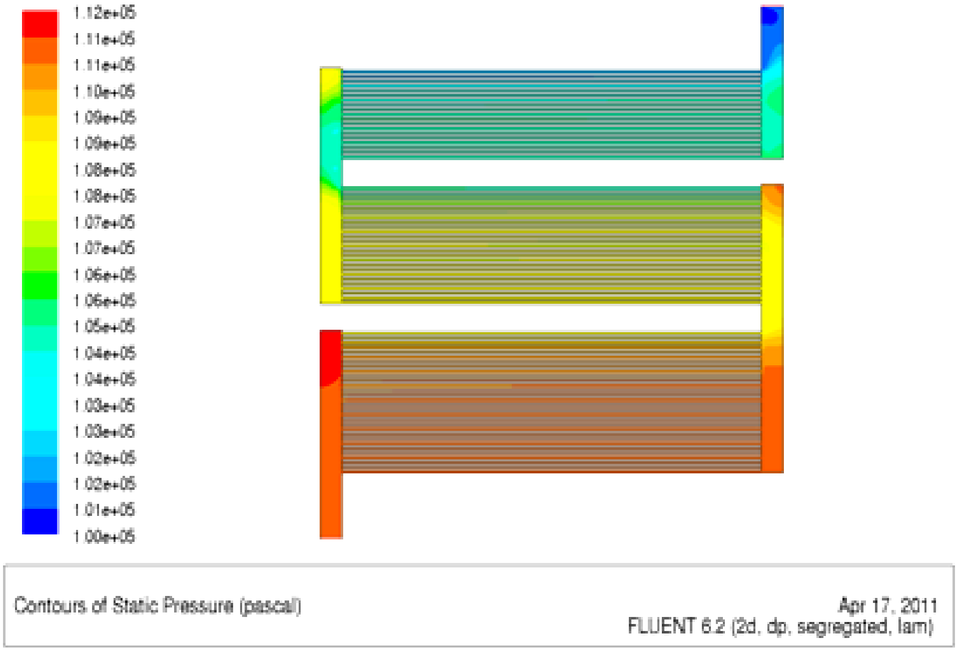

Figure 6.3: Pressure contour for three stages of the ED stack using Fluent

6.4 Experimental and CFD Results for Single Compartment of ED Stack

As discussed above that due non-transparent component like membranes, it is very difficult to visualise the flow inside compartment of the ED stack. Thus, an experimental set up was developed and discussed in detail in chapter 4. The flow inside the compartment has been observed experimentally by injecting the colour die. Apart from that the CFD was used to compute the velocity and pressure at different locations in the compartment. Also the flow behaviour results in the compartment were computed using CFD and are presented in the following sections.

6.4.1 Flow Pattern inside the Compartment (Experimental results)

The experimental procedure to visualize the flow inside the compartment is discussed in Chapter 4, at the time of experimentation photographs of the compartment were captured after appropriate time interval and are presented in Fig.6.4(a-d). Initially, the compartment was fed with water. It was very difficult to visualize the live flow inside the compartment. To overcome this problem, the flow of water was stopped and dark pink coloured solution was passed (due care was take no air pockets will get developed).

Immediately after the supply of coloured solution photograph was captured and presented in Fig.6.4(a). It shows a clear flow of coloured solution from both the inlets made at one side of compartment. It can be observed from Fig.6.4(b and c) that after some time interval the flow velocity of the coloured solution is maximum along the length of the compartment. However, the coloured solution gets spread in the perpendicular direction of flow. As the coloured solution reaches at the other end of compartment and flows through the outlets around 80 percent area of the compartment gets occupied with coloured solution that is shown in Fig.6.4(d). However, the maximum flow velocity in the compartment may be in the middle section and this may reduces the effective area of membrane.

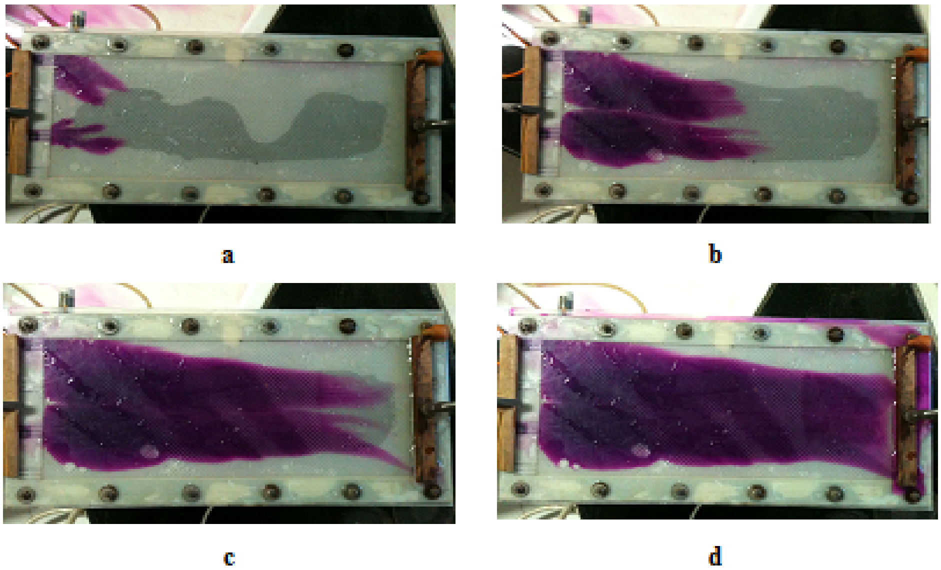

Figure 6.4: Flow visualization in the existing compartment of ED stack

6.4.2 Flow Analysis of the Compartment using CFD

Experimentally it is difficult to measure the velocity and pressure at different locations inside the compartment. First, middle (where velocity at outlet increasing from zero) and last compartment of the first stage were taken for the simulation and contours are generated for the velocity and pressure. As per the assumptions and boundary condition given in previous chapter the velocity and pressure contours for the compartment were computed using Navier-Stroke equations. The velocity and Pressure contours of the compartments of first stage were generated using FLUENT and are presented in Figs.6.5-6.7

The velocity and pressure contours of the first compartment of the first stage were analysed and are presented in Fig.6.5(a-c).The velocity contour of the first compartment (Fig.6.5(a)) shows that the flow velocity at the inlet of compartment is higher and decreases continuously along the length of the compartment. The graphical presentation of velocity magnitude along the length of compartment is given in Fig.6.5(b). It is observed that velocity tends to decrease in the first compartment from 0.03 m/s (at inlet) to 0.01 m/s (to outlet) which tends to zero velocity at the outlet. While the pressure magnitude Fig.6.5(c) shows constant pressure (110777 N/m2) inside the compartment across the length of compartment. This shows that no pressure drop along the length of compartment, thus flow will not occur in the first compartment. This is well in the agreement with the results obtained for ED stack as presented in Fig.6.1(c and d) and Fig.6.2for the ED stack.

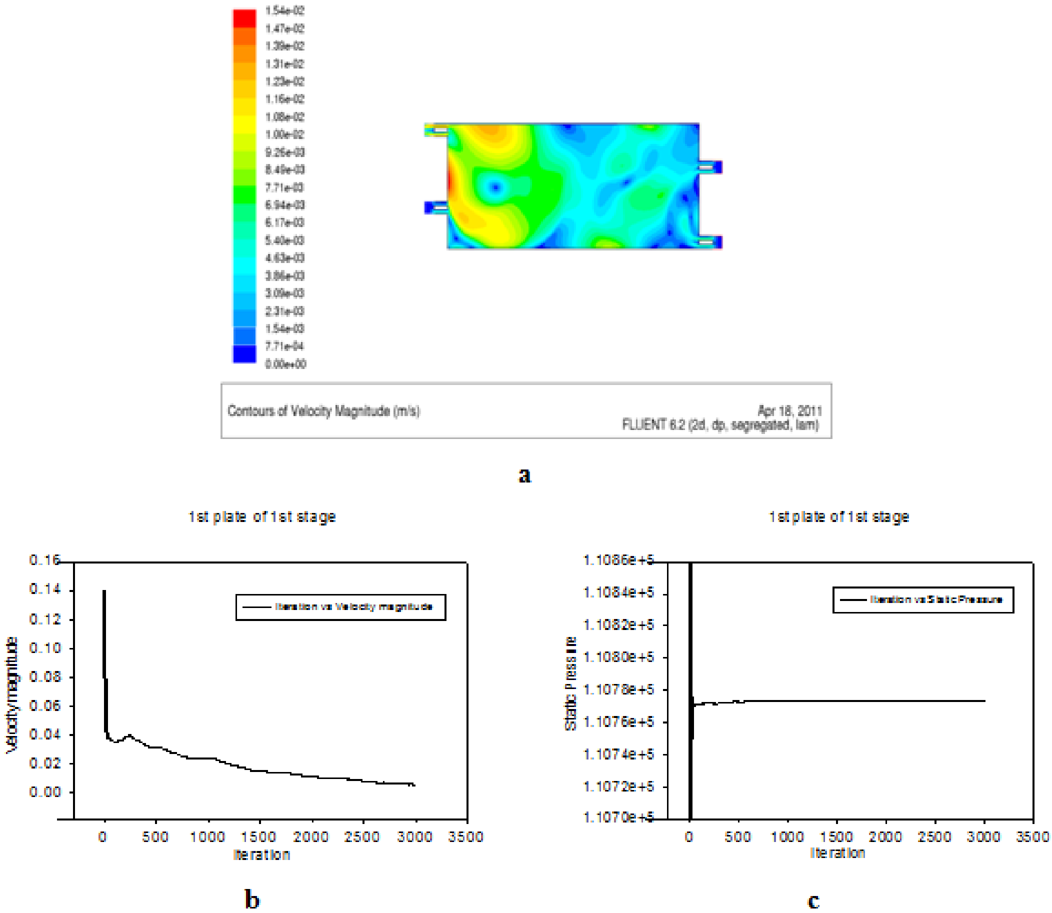

Figure 6.5: Velocity contour for first compartment of the first stage

Similarly, the velocity and pressure contours of the middle compartment of the first stage were analysed and are presented in Fig.6.6(a-c). The velocity contours of the middle compartment (Fig.6.6(a)) shows that the flow velocity increases from the inlet to outlet inside the compartment, however few pockets of zero velocity are observed. The velocity magnitude along the length of compartment is graphically presented in Fig.6.6(b). It is observed that velocity tends to increase from 0.2 m/s (at inlet) to 0.45 m/s (at outlet). While the pressure magnitude Fig.6.6(c) shows constant decrease in pressure along the length of compartment. Both the velocity and pressure magnitudes reveal the continuous flow of water is inside the compartment.

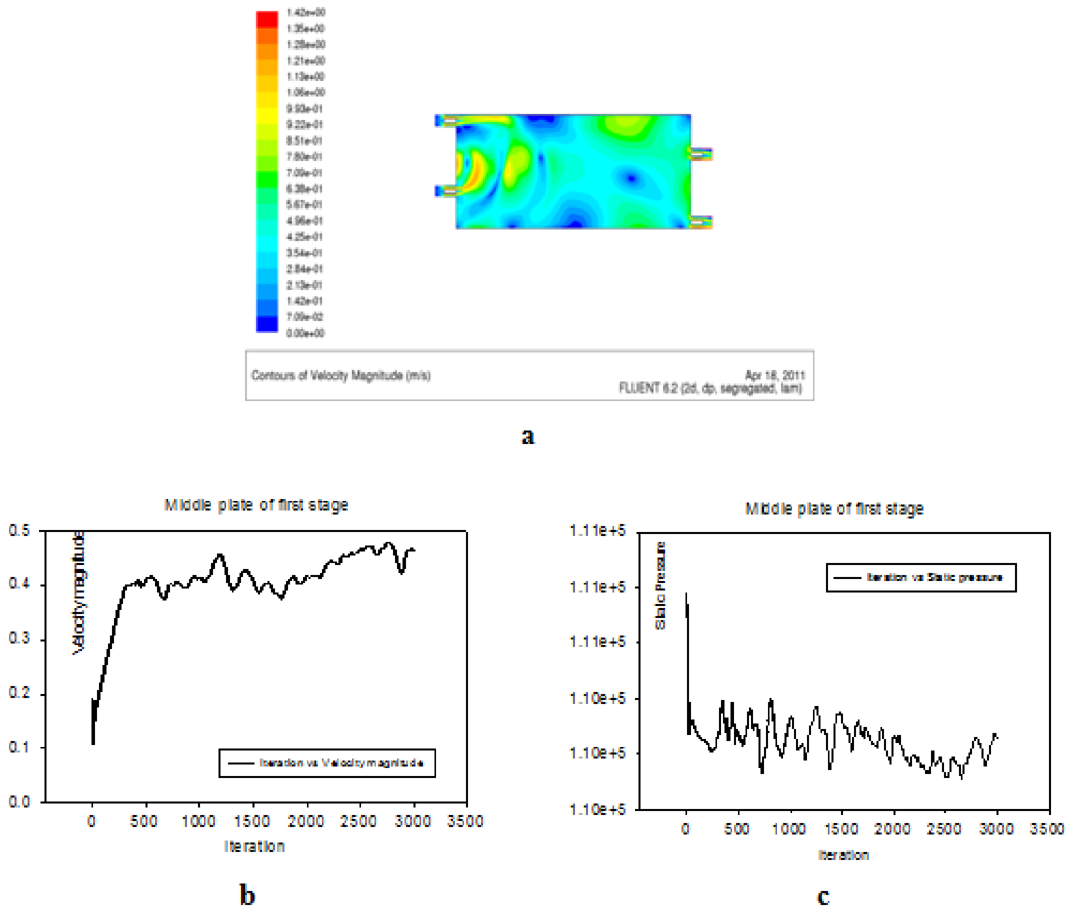

Figure 6.6: Velocity contour for middle compartment of the first stage

Similarly, the velocity and pressure contours of the last compartment of the first stage were analysed and are presented in Fig.6.7(a-c). The velocity contours of the last compartment Fig.6.7(a) shows that the flow velocity increases from the inlet to outlet inside the compartment, however few pockets of zero velocity are observed. The velocity magnitude along the length of compartment is graphically presented in Fig.6.7(b). It is observed that velocity tends to increase from 0.2 m/s (at inlet) to 0.7 m/s (at outlet). While the pressure magnitude Fig.6.7(c) shows constant decrease in pressure along the length of compartment. Both the velocity and pressure magnitudes reveal the continuous flow of water is inside the compartment.

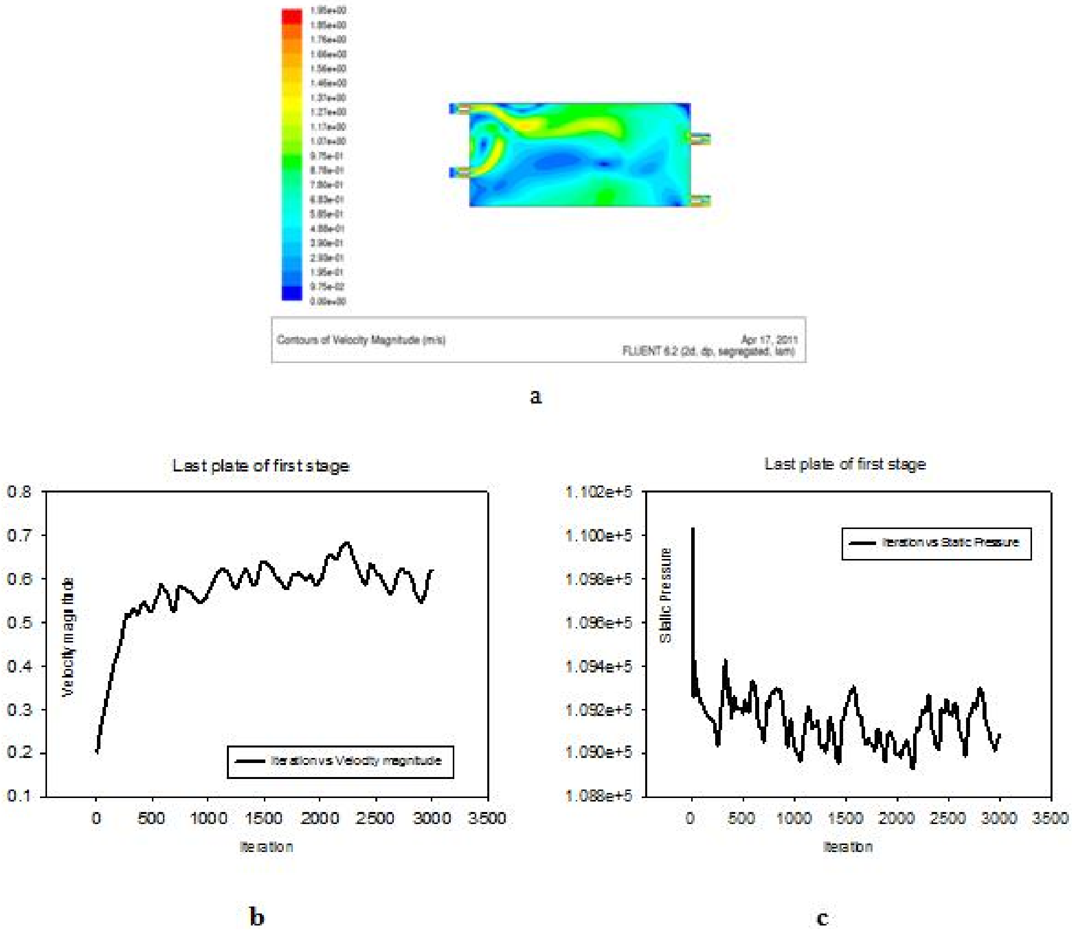

Figure 6.7: Velocity contour for last compartment of the first stage

In summary, it is observed that the flow velocity in the first compartment of first stage is continuously decreasing and at the outlet of compartment becomes zero.

This shows that the compartment is without any flow of water i.e. the water is stagnant in this compartment. This can be also confirmed from Fig.6.2 that most of the initial compartments in the first stage are stagnant. While the analysis of middle compartment shows that the velocity at the outlet is slightly higher and water is continuously flowing through the middle compartments of first stage and same can be confirm from Fig.6.2. Similarly, the last compartment of the first stage is having higher velocity than the compartments located in the middle part of the first stage.

6.5 Proposed Design of the Compartment and ED Stack:

The velocity, pressure and flow analysis of the existing compartments of the ED stack have been discussed in detail in the above section. From the results of the compartment and the flow through the Ed stack, it can be concluded that the water flow is not equally distributed in the compartments of the Ed stack. Most of the compartments in the lower region of all the stages are stagnant. Also from the experimental analysis of individual compartments, it is observed that zero velocity pockets were observed which reduces the effective area of membrane for transport of ions.
In summary, the efficiency of the ED stack decreases due to both non uniform flow through the compartments (stagnation of the compartments) and water if finding least resistant path to flow inside the compartment (reduces the effective area of membrane). Thus to increase the performance of the Ed stack, new designs are proposed for both ED stack inlet header and individual compartment inlet and outlet openings.

6.5.1 Trapezoidal Inlet Header for ED stack:

For equal distribution of water flow through all the compartments of the ED stack, it is proposed to change the geometry of the inlet header for all the stages. It was difficult to fabricate the experimental model with in stipulated time, only CFD methodology is adopted for analysis of proposed design.

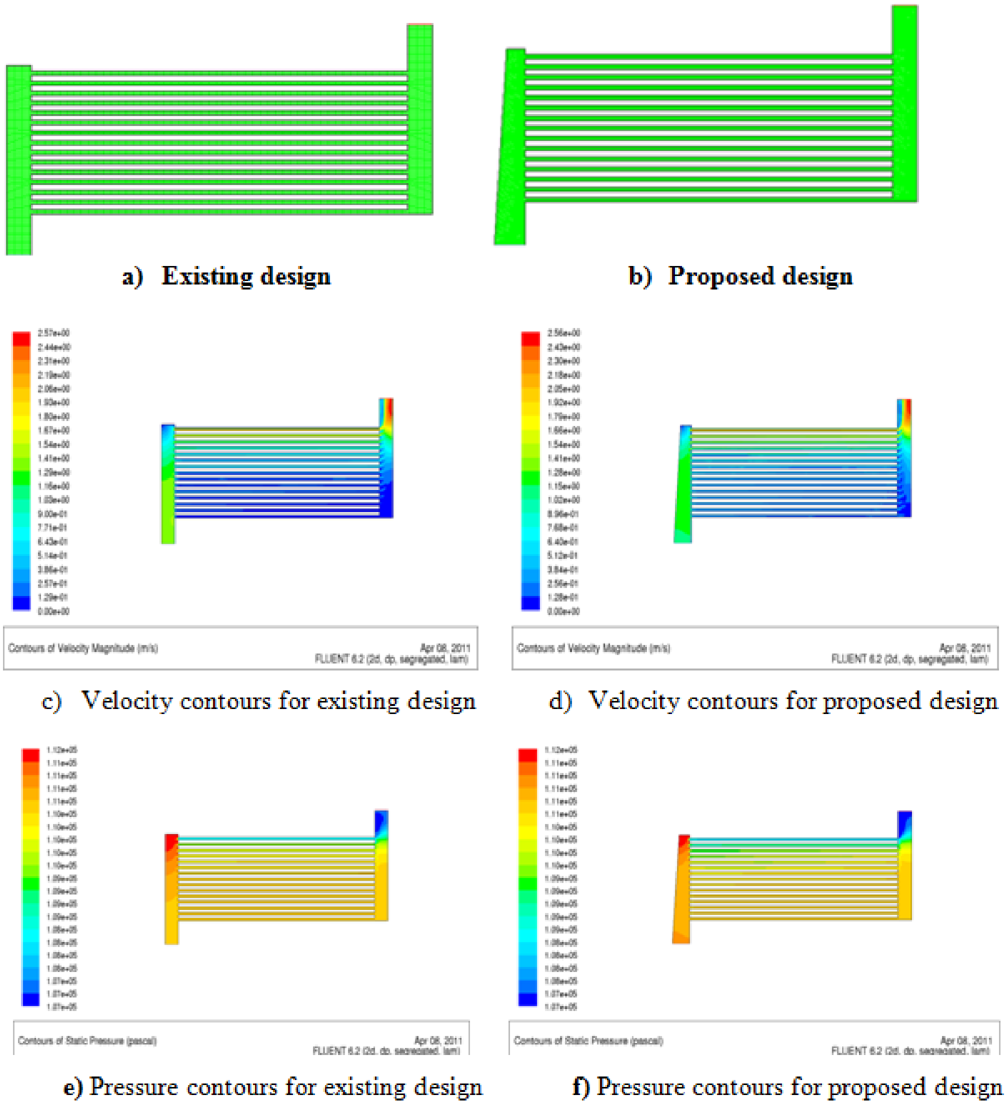

Figure 6.8: Velocity and pressure contours for existing and proposed designs of ED stack

Thus the geometries of the inlet header of the first stage for existing and proposed trapezoidal are given in Fig.6.8(a and b). Further CFD tool was used to study the flow patterns. The results of the proposed design are compared with the existing design of the inlet header.

The velocity and pressure contours for existing and proposed designs for first stage are presented in Fig.6.8(c-f). It is observed from Fig.6.8(c) that the flow through the most of lower side compartments is stagnant and the velocity in the outlet header approaches to zero. The similar results are also reported in Fig.6.2. While the velocity contours for the new proposed design are presented in Fig.6.8(d). It is observed that the improvement in the velocity at the lower section of the outlet header compare to the existing design. Hence the flow occurs through the all compartments of the new proposed design. Similar results for pressure contours are observed and presented in Fig.6.8(e and f), where the pressure continuously decreases from inlet to outlet of the compartment with new proposed design.

6.5.2 Flow Pattern inside the Proposed Compartments (Experimental results)

The visual observations of the existing compartment are shown in Fig.6.4(a-d). Similarly, the experiments with new proposed inlet and outlet openings were conducted and the photographs captured are presented in Fig.6.9(a-d). Thus the comparison of Fig.6.4(a-d) and Plate Fig.6.9(a-d) shows that the flow velocity of the coloured solution is maximum along the length of the compartment and similarly gets equally spread in lateral direction with the proposed design of the compartment. Thus the flow behaviour in the proposed design is better than the existing one because of equal distribution of inlet and outlet openings and the angular opening of inlets which increases the velocity vector in the perpendicular to the length of the compartment.

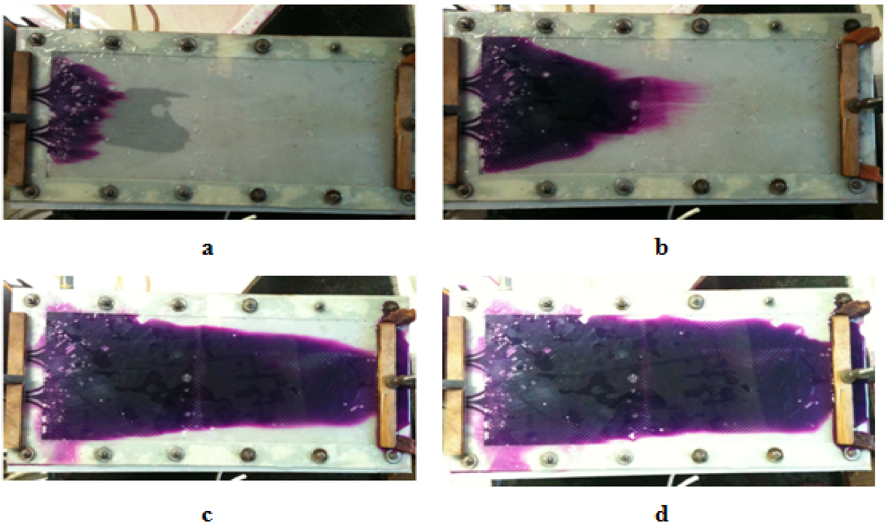

Figure 6.9: Flow visualization in the proposed compartment of ED stack

6.5.3 Flow Analysis of the Proposed Compartment using CFD

The velocity contours along with velocity magnitudes of the last compartments of all three stages for existing and new proposed design are presented in Figs.6.10 -6.12. The velocity contours of the last compartments of first, second and third stages are presented in Fig.6.10(a), Fig.6.11(a) and Fig.6.12(a), respectively. It is observed that the flow velocity of existing design in all three compartments is higher compare to the respective proposed design compartments as shown in Fig.6.10(b), Fig.6.11(b) and Fig.6.12(b).

Also from the velocity magnitude for existing and proposed compartments is graphically presented in Fig.6.10(c), Fig.6.11(c) and Fig.6.12(c). The velocity in the existing last compartment of all three stages is around 0.6 m/s, 0.8 m/s and 0.9 m/s, while it is observed around 0.3 m/s, 0.4 m/s and 0.5 m/s for the proposed last compartments of first, second and third stages, respectively. Thus it can be concluded that the velocity in the last compartments of all stages of the existing ED stack is nearly double than the velocity in the compartments of proposed design. This shows that the maximum area in the compartment is covered with moderate velocity. Thus this increases the effective area of the membrane and may enhance the efficiency of the ED stack.

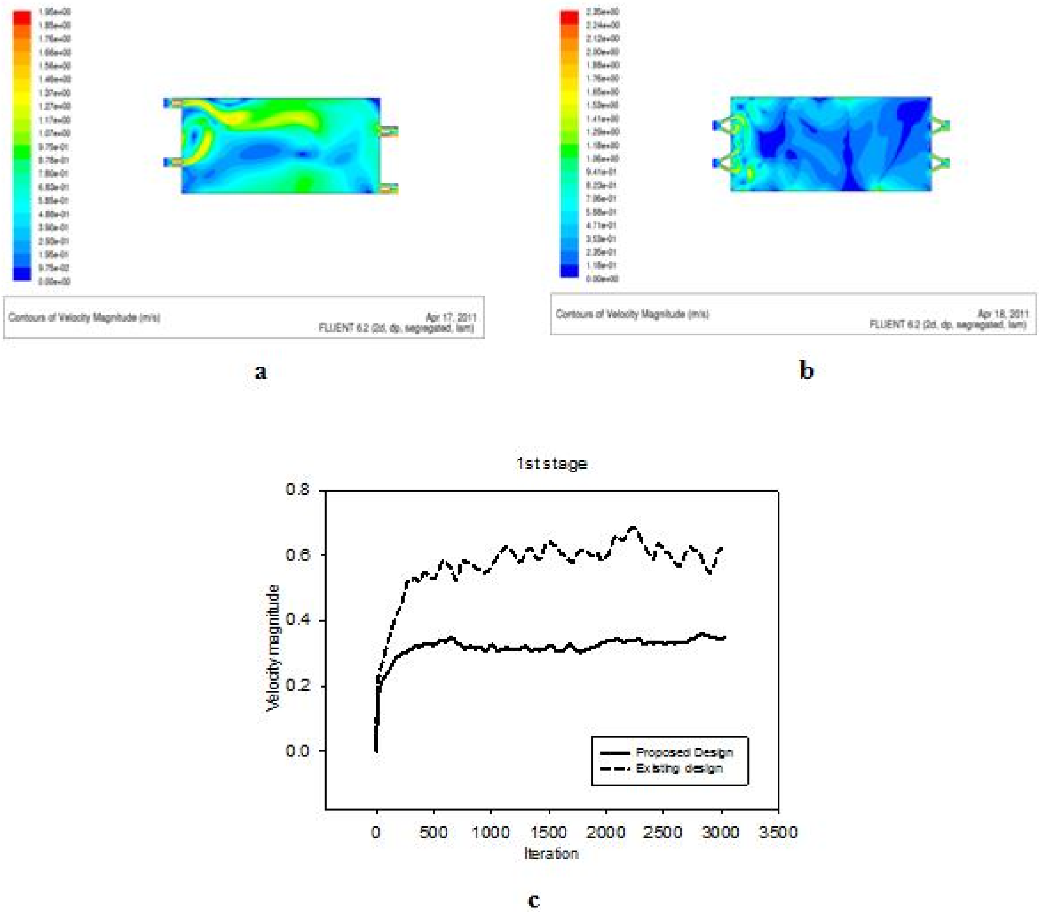

Figure 6.10: Velocity and pressure contours for last compartment of the first stage

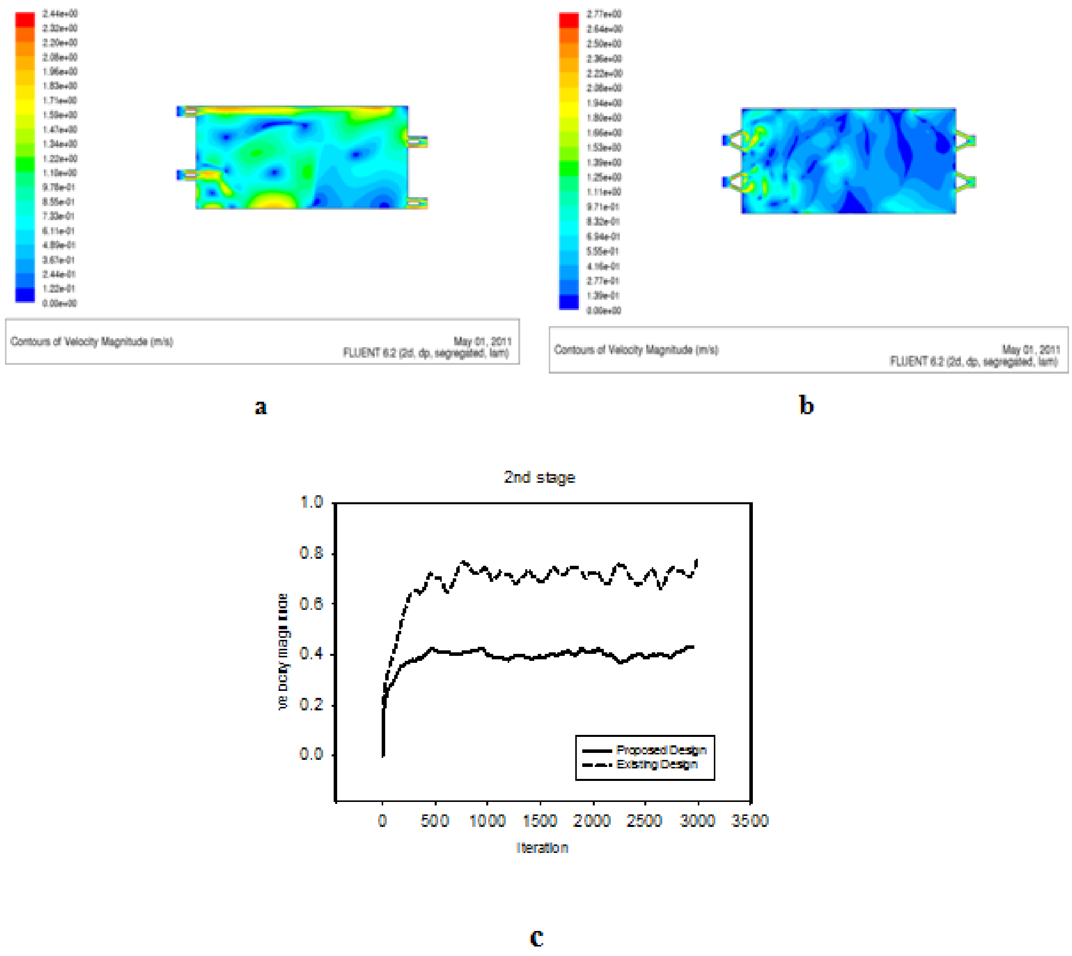

Figure 6.11: Velocity and pressure contours for last compartment of the Second stage

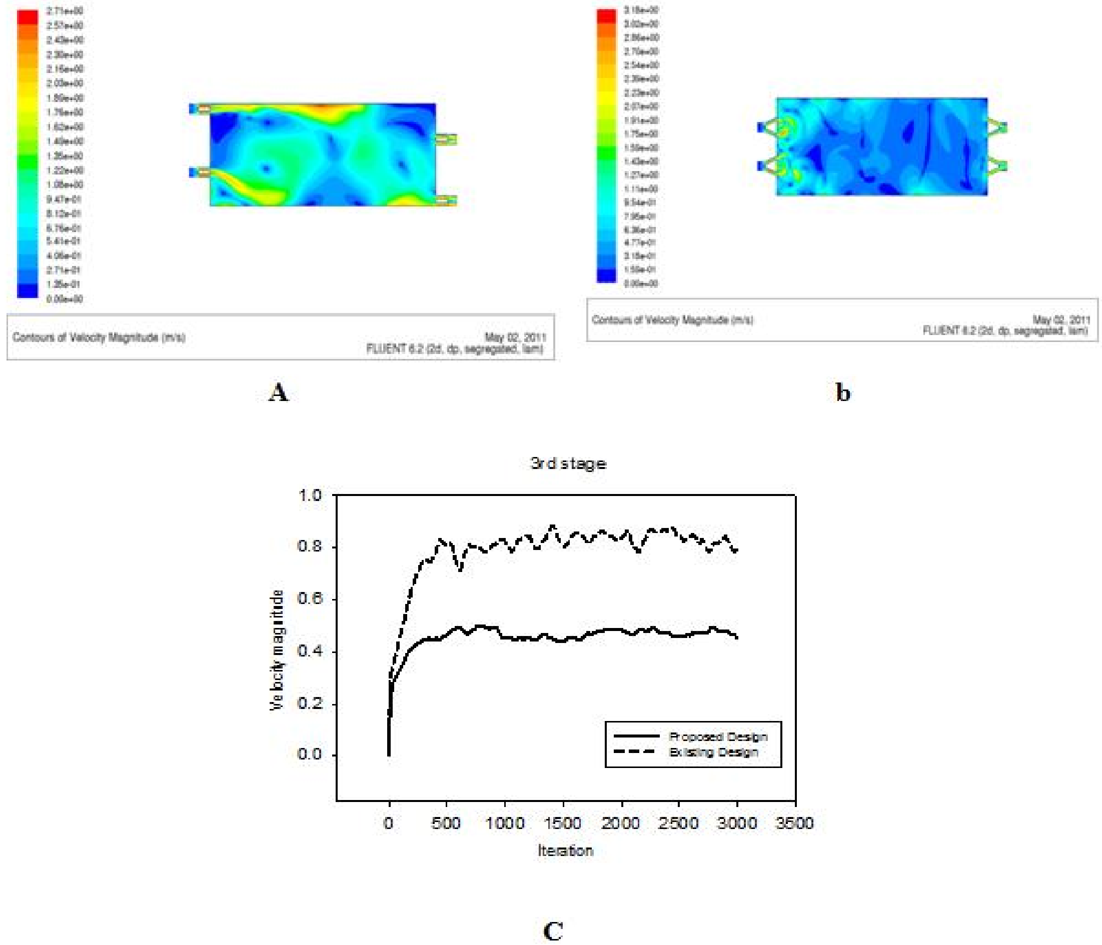

Figure 6.12: Velocity and pressure contours for last compartment of the third stage

Chapter 7

Conclusion

7.1 Concluding Remarks

The ED stack is generally used in various industrial processes namely, water purification, effluent treatment, desalination of chemicals, recovery of valuable chemicals, etc. As per the industries requirements the design of the ED stack varies significantly for its effective use. The compartments are formed by alternate arrangement of cation and anion exchange membranes. The arrangement of compartments in parallel and group of parallel compartments in series is preferred for handling huge amount liquid in the ED stacks. Thus the arrangement of compartment plays vital role for equal distribution of liquid in the compartments. Apart from this the geometries of the inlet and outlet openings of the compartment for liquid flow also plays important role to decide the effective area of membrane and thus affects the performance of ED stack. Thus to improve the performance of the ED stack efforts have been made experimentally and using the CFD methodology for the analysis of flow inside the compartments of the ED stack. Boundary conditions for the present investigations are decided based on the experimental results. The simulation techniques available with FLUENT based on Navier-stokes code is used to compute the flow characteristics of the compartments. Based on the experimental results, theoretical calculations and CFD analysis following conclusions can be drawn.

a. The velocity at the inlet and outlet points of the compartment predicted using CFD is well in agreement with the theoretically results. However, large variations in velocities inside the compartment area are observed between results obtained by CFD and theoretically. As the equal mass flow rate from all the compartments was consider during the theoretical calculations, while in CFD the velocities in the compartment areas was calculated using the available codes. The visual flow observations in the compartment are also well in agreement with CFD results.

b. Based on the results of existing ED stack, new proposed design for the inlet header is proposed which flow velocities through all compartments is in narrow range. This reveals that the flow is through all the compartments and less chances of stagnation of liquid in the compartments.

c. Similarly, for better flow distribution inside the compartment new proposed inlet and outlet opening are proposed. This increases the effective membrane area of the compartment which enhances the transport of ions and thus increases the performance of the ED stack.

d. Based on these conclusions it can be summarized that the proposed designs in the ED stack and in openings of compartment can either reduce the size of ED stack which reduces the initial capital cost and maintenance cost or enhances the performance of the stack.

7.2 Future Scope of Work

The present problem requires good understanding of CEDI unit with its flow arrangement and fluid mechanics involved. In the present investigation, flow characteristics for only treated compartment are analyzed using FLUENT. The following studies need to address the problems associated with ED stack with greater attention for detail and systematic approach require for its cost effectiveness.

- Two dimensional approaches is used in the present investigation, additional efforts are required to solve the problem with three dimensional mode.
- The flow characteristics for both treated and rejected compartments may be carried out with their common consequence on the ED stack.
- The compartments parallel and series arrangements like number of parallel compartments and number of stages can be changed to minimize the stagnant compartment.
- Mathematical model can be developed for optimization of the numbers of compartments and stages.

References

[1] P. Ray S.K. Adhikary, J.M. Gohil. Studies on the resistance developed at different stages in an electrodialysis stack operated in parallel-cum-series flow pattern. *Journal of Membrane Science (245)*, pages 131–136, 2004.

[2] K.A Patel. Analysis of water flow inside the compartment of continuous cedi unit using cfd.

[3] *Fluent 6.2 user,s guide.* ansys corporation, 2002.

[4] N.P.Kotsupalo A.D.Ryabstev and V.I.Titarenko. Development of a two-stage electrodialysis set-up for economical desalination of sea-type artesian and surface waters. *Desalination (137)*, pages 207–214, (2001).

[5] Sirkar K.K Winston Ho W.S. *Membrane Handbook.* Champan Hall, 1992.

[6] Yoshinobu Tanaka. A computer simulation of continuous ion exchange membrane electrodialysis for desalination of saline water. *Desalination 249*, pages 809–821, (2009).

[7] Rockstraw D. A.; Scamehor J. F. Use of electrodialysis to remove acid, salt, and heavy metal mixtures from aqueous solutions.

[8] Carl-Ola Danielsson. Analysis of water flow inside.

[9] J.P. Chiou A.C. Mueller. Review of various types of flow maldistribution in heat exchangers. *Heat Transfer Engineering 9*, pages 356–50, 1988.

[10] S.K. Lang A.E. Bergles S. Lalot, P. Florent. Flow maldistribution in heat exchangers. *Applied Thermal Engineering 19 (8)*, pages 847–863, 1999.

[11] J.M. Robertson J.B. Kitto Jr. Effects of maldistribution of flow on heat transfer equipment performance. *Heat Transfer Engineering 10*, pages 18–25, 1989.

[12] B. Sunden F.A. Tereda, N. Srihari. Experimental investigation on port-to-channel flow maldistribution in plate heat exchangers. *Heat Transfer Eng. 28 (5)*, pages 435–443, 2007.

[13] S.K. Das P.R. Bobbili, B. Sunden. Thermal analysis of plate condensers in presence of flow maldistribution. *Int. J. Heat Mass Transfer 49*, pages 4966–4977, 2006.

[14] S.K. Das P.R. Bobbili, B. Sunden. An experimental investigation of the port flow maldistribution in small and large plate package heat exchangers. *Appl. Thermal Eng. 26 (16)*, pages 1919–1926, 2006.

[15] A.M. Zhou K. Zhang J. Wang Y.Z. Li, J. Wen. Piv experimental investigation of entrance configuration on flow maldistribution in plate-fin heat exchanger. *Cryogenics 46 (1)*, pages 37–48, 2006.

[16] S.K. Das B.P. Rao, B. Sunden. An experimental and theoretical investigation of the effect of flow maldistribution on the thermal performance of plate heat exchangers. *J. Heat Transfer Trans. ASME 127 (3)*, pages 332–343, 2005.

[17] A. Jiao S. Baek. Effects of distributor configuration on flow maldistribution in plate-fin heat exchangers. *Heat Transfer 26 (4)*, pages 19–25, 2005.

[18] S.K. Das B.P. Rao. An experimental study on the influence of flow maldistribution on the pressure drop across a plate heat exchanger. *J Fluids Eng. Trans. ASME 126 (4)*, pages 680–691, 2004.

[19] Q. Xu Z. Zhang, Y.Z. Li. Experimental research on flow maldistribution in platefin heat exchangers. *Chin. J. Chem. Eng. 12 (1)*, pages 7–13, 2004.

[20] C.Z. Chen R. Zhang A.J. Jiao, Y.Z. Li. Experimental investigation on fluid flow maldistribution in plate-fin heat exchangers. *Heat Transfer Eng. 24 (4)*, pages 25–31, 2003.

[21] S.A. Jeong A.J. Jiao, R. Zhang. Experimental investigation of header configuration on flow maldistribution in plate-fin heat exchanger. *Appl. Thermal Eng. 23 (10)*, pages 1235–1246, 2003.

[22] H.A.K.S. Al-Janabi M.A.R.S. Al-Baghdadi. Effect of operating parameters on the hygro-thermal stresses in proton exchange membranes of fuel cells. *Int. J.Hydrogen Energy 32*, pages 4510–4522, 2007.

[23] J. St-Pierre D.P. Wilkinson S.D. Knights, K.M. Colbow. Aging mechanisms and lifetime of pefc and dmfc. *J. Power Sources 127*, pages 127–134, 2004.

[24] R.M. Darling J.P. Meyers. Model of carbon corrosion in pem fuel cells. *J. Electrochem. Soc. 153*, pages A1432–A1442, 2006.

[25] J.W. van Zee S. Dutta, S. Shimpalee. Three-dimensional numerical simulation of straight channel pem fuel cells. *J. Appl. Electrochem 30*, pages 135–146, 2000.

[26] J.W. van Zee S. Dutta, S. Shimpalee. Numerical prediction of mass exchange between cathode and anode channels in a pem fuel cell. *Int. J. Heat Mass Transfer 44*, pages 2029–2042, 2001.

[27] S.H. Chan T.C. Jen, T. Tan. Chemical reacting transport phenomena in a pem fuel cell. *Int. J. Heat Mass Transfer 46*, pages 4157–4168, 2003.

[28] R.G. Reddy A.Kumar. Effect of channel dimensions and shape in the flow field distributor on the performance of polymer electrolyte membrane fuel cells. *J.Power Sources 113*, pages 11–18, 2003.

[29] R.G. Reddy A.Kumar. Modeling of polymer electrolyte membrane fuel cell with metal foam in the flow field of the bipolar/end plates. *J. Power Sources 114*, pages 54–62, 2003.

[30] D. Poulikakos S.M. Senn. Polymer electrolyte fuel cells with porous materials as fluid distributor and comparisons with traditional channeled systems. *J.Heat Transfer Trans. ASME 126*, pages 410–418, 2004.

[31] C. Bautista P.L. Garcia-Ybarra L. Daza E. Hontanon, M.J. Escudero. Optimization of flow-field in polymer electrolyte membrane fuel cells using computational fluid dynamics techniques. *J. Power Sources 86*, pages 363–368, 2000.

[32] L. Valino C. Marin-A. Pascau F. Barreras, A. Lozano. Flow distribution in a bipolar plate of a proton exchange membrane fuel cell: experiments and numerical simulation studies. *J. Power Sources 144*, pages 54–66, 2005.

[33] L. Valino R. Mustata-C. Martin F. Barreras, A. Lozano. Fluid dynamics performance of different bipolar plates, part i. velocity and pressure fields. *J.Power Sources 175*, pages 841–850, 2008.

[34] C.Y. Wang S. Um. Three-dimensional analysis of transport and electrochemical reactions in polymer electrolyte fuel cells. *J. Power Sources 125*, pages 40–51, 2004.

[35] S. Chen Y. Liu-K. Cen G. Hu, J. Fan. Three-dimensional numerical analysis of proton exchange membrane fuel cells (pemfcs) with conventional and interdigitated flow fields. *J. Power Sources 136*, pages 1–9, 2004.

[36] M. Vynnycky E. Birgersson. A quantitative study of the effect of flowdistributor geometry in the cathode of a pem fuel cell. *J. Power Sources 153*, pages 76–88, 2006.

[37] S. Srinivasan P. Costamagna. Quantum jumps in the pemfc science, technology from the 1960s to the year 2000: part ii. engineering, technology development and application aspects. *J. Power Sources 102*, pages 253–269, 2001.

[38] R. Harwoth K. Hertwig, L. Martens. Mathematical modeling and simulation of polymer electrolyte membrane fuel cells. part i: model structures and solving an isothermal one-cell model. *Fuel Cells 2*, pages 61–77, 2002.

[39] K.D. Sarit S. Pandiyan-N. Rajalakshmi K.S. Dhathathreyan M.B. Ganesh, R. Prabhakar. Analysis of flow maldistribution for fuel and oxidant in a pemfc. *J. Energy Resources Technol. Trans. ASME 126*, pages 262–270, 2004.

[40] T.R. Kumar B. Muralidhar A.S. Bansode, S. Patel. Numerical simulation of effects of flow maldistribution on heat and mass transfer in a pem fuel cell stack. *Heat Mass Transfer 43*, pages 1037–1047, 2007.

[41] C.G. Lee Y.S. Yoo-H.C. Lim J.H. Koh, H.K. Seo. Pressure and flow distribution in internal gas manifolds of a fuel-cell stack. *J. Power Sources 115*, pages 54–65, 2003.

[42] S.-C. Yen C.-H. Chen, S.-P. Jung. Flow distribution in the manifold of pem fuel cell stack. *J. Power Sources 173*, pages 249–263, 2007.

[43] R.M. Darling T.W. Patterson. Damage to the cathode catalyst of a pem fuel cell caused by localized fuel starvation. *Electrochem. Solid-State Lett. 9*, pages A183–A185, 2006.

[44] N. Kimiaie J. Mergel M. Muler H. Dole, R. Jung. Interaction between the diffusion layer and the flow filed of polymer electrolyte fuel cells - experiments and simulation studies. *J. Power Sources 124*, page 371384, 2003.

[45] J.J. Baschuk T. Kanezaki, X. Li. Cross-leakage flow between adjacent flow channels in pem fuel cells. *Power Sources 162*, page 415425, 2006.

[46] Anderson Jhon D. *Computational Fluid Dynamic the basic with applications.* Mc Graw-Hill International Edition, 1998.

[47] H. K Versting and W.Malasekera. *An Introduction to computional Fluid Dynamics.* Longman Scientific and Technical Publication, 1995.

[48] J.H Ferziger and M.Peric. *Computational method for fluid dynamics.* Springer (India) Private Limited,New Delhi, 2004.

[49] Acheson.D. *Elementary Fluid Dynamics.* Claredon Press, Oxford, 1990.

[50] D.snita K.Bouzek R.Kodym, F.vlasak. Spatially two-dimensional mathematical model of flow hydrodynamics in a channel filled with a net-like spacer. *Membrane science*, pages 171–183, 2010.